

# Visualizing High-Dimensional Graph Embeddings via Informed Multi-View Projections

Ya Ji , Xuefeng Li , Timo Brand , Jacob Miller , Peng Zhang , Stephen Kobourov , and Yifan Hu 

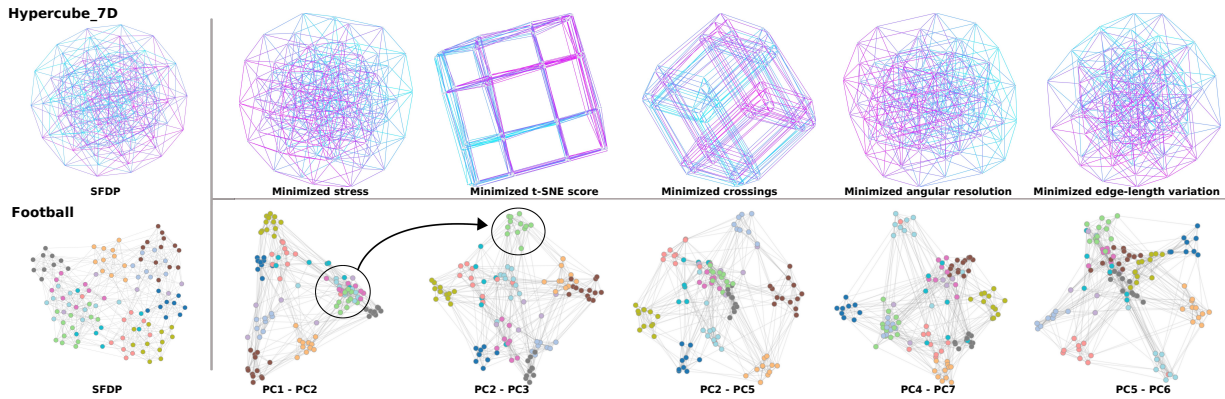


Fig. 1: Example visualizations produced from high-dimensional projections. (Top) shows a 7D hypercube embedded via `sfdp` in 10D and projected to optimize stress, t-SNE score, edge crossings, angular resolution, and edge length variance, respectively. (Bottom) shows the classic football network embedded via a spectral embedding in 10 dimensions, from five different axis-aligned viewpoints. The set of projections reveals that class memberships are spatially salient in some projections and disappear in others, highlighted by the circled cluster in the first two projections.

**Abstract**— Graphs are commonly visualized in 2D, where humans readily interpret spatial relationships, yet such layouts often distort higher-dimensional structure. We propose to embed graphs in high-dimensional space and search for informative 2D viewpoints that optimize aesthetic and readability metrics (e.g., edge crossings and angular resolution), enabled by a novel differentiable surrogate for edge crossings. Numerical experiments show that these viewpoints consistently outperform standard 2D layouts, and can even surpass methods explicitly designed to optimize these metrics. We further introduce `DataFly`, an interactive system for exploring multiple candidate viewpoints through seamless navigation. A usability study demonstrates that our approach reveals structural patterns that remain hidden in conventional 2D visualizations.

**Index Terms**—Graph visualization, dimension reduction

## 1 INTRODUCTION

Graph visualization converts abstract relationships into readable graphics, enabling users to understand complex relational data, uncover patterns, and make informed decisions. Traditionally, graphs are visualized in 2D, reflecting human-interpretable spatial relationships. However, large real-world graphs often exhibit characteristics reminiscent of high-dimensional data: the small-world phenomenon, in which most node pairs are connected by short paths, mirrors the distance concentration observed in high dimensions, and real-world graphs, like high-dimensional point clouds, tend to be locally dense and globally sparse. Two-dimensional layouts struggle to preserve these higher-dimensional relationships. Just as a cube cannot be projected onto a 2D plane with equal edge lengths, complex networks contain local connectivity patterns, such as dense cliques or overlapping communities, that no single 2D projection can faithfully represent. It follows that a single 2D graph layout, although intuitive and accessible, risks distorting or obscuring the higher-dimensional structure of the data.

However, high-dimensional layouts introduce a practical challenge: presenting them to human readers requires choosing a 2D projection, or viewpoint, at any given time. Thus, high-quality viewpoints are necessary for high-dimensional layouts to be effective visualization

tools, but this has received limited exploration in the literature. Many methods rely on computing a single projection that is optimal under some criteria [25, 43, 65]. Van Wageningen et al. [62] investigate the viewpoint problem in the context of 3D drawings, but it remains unclear whether effective projections of higher-dimensional layouts can be achieved.

These observations motivate the following research question: *Do high-dimensional graph embeddings contain 2D projections that reveal structural patterns otherwise obscured by traditional static layouts?* To investigate this, we develop a computational pipeline to systematically explore high-dimensional graph layouts, which produces a family of candidate projections. We further introduce a gradient-based optimization scheme that finds near-optimal projections for a given quality metric, such as stress, edge crossings, or angular resolution. Our findings show that such projections can outperform state-of-the-art algorithms that are explicitly designed to optimize these same metrics directly in 2D. Throughout the paper, we use the term *optimal projection* as shorthand for the result of this gradient-based optimization, noting that it converges to a local rather than global optimum.

To make these high-dimensional embeddings accessible and explorable, we provide `DataFly`, an interactive online tool for real-time visualization of high-dimensional graph layouts. `DataFly` enables principled exploration of viewpoints: users can inspect optimal projections for specific metrics, or transition between them by “flying over” the high-dimensional space, observing how one projection morphs into another. Because all viewpoints derive from a single shared embedding, diverse visual perspectives on the same network coexist within a coherent spatial structure, allowing users to discover structural patterns that remain hidden in any single 2D layout.

- Ya Ji, Xuefeng Li, Peng Zhang and Yifan Hu are with the Khoury College of Computer Sciences, Northeastern University, Seattle, WA, USA. E-mail: {ji.ya1 | li.xuefeng | zhang.peng2, yif.hu}@northeastern.edu.
- Timo Brand, Jacob Miller and Stephen Kobourov are with the School of Computation, Information and Technology, Technical University of Munich, Heilbronn, Germany. E-mail: {timo.brand | jacob.miller | stephen.kobourov}@tum.de.

Our main contributions are as follows:

- We show that the optimal 2D projection of a high-dimensional graph embedding can yield better metric values than several state-of-the-art benchmarks that optimize such metrics directly in 2D.
- We propose an differentiable loss function, SigmoidX, which enables the effective minimization of edge crossings, and demonstrate that the optimal projection using this loss function achieves significantly fewer crossings than  $SGD^2$  and SmartGD.
- We provide a working prototype of DataFly, an interactive system for exploring high-dimensional graph layouts and identifying viewpoints of interest, evaluated by a small usability study with both expert and non-expert participants.

While our primary focus is on visualizing graph data with straight-line node-link diagrams, the name DataFly reflects the fact that our interactive multi-view exploration approach naturally extends to general high-dimensional data. A video of the system in action can be found at <http://tiny.cc/datafly-video>. DataFly is made publicly available at <https://datafly.algo.cit.tum.de>.

In the remainder of the paper, DataFly refers to both the interactive system and the associated optimal-projection framework.

## 2 RELATED WORK

Since 1963 [61], numerous graph drawing algorithms have been proposed. A widely used class of methods for generating straight-line drawings relies on physical models that minimize the energy of the system. Examples include stress-based models, which minimize the stress energy of springs connecting nodes [26, 40, 67], and force-directed systems of springs and electrical charges, in which springs along edges contract while electrical charges on nodes repel each other [20, 23, 42].

### 2.1 Layout algorithms for optimizing specific metrics

There are a number of layout methods that specifically target aesthetic metrics, such as minimizing edge crossings [17, 55], maximizing crossing angles [2, 5], or a combination [18]. Two notable algorithms are  $SGD^2$  [1] and SmartGD [64].

$SGD^2$  is a method that can jointly optimize multiple graph readability criteria. In particular, it can optimize any criterion that can be described by a differentiable function. When a criterion is not a differentiable function (e.g., edge crossings), a proxy objective is used instead.  $SGD^2$  supports optimization of angular resolution, edge crossings, and desired edge lengths, among other criteria. SmartGD [64] is a deep-learning framework for graph drawing based on generative adversarial networks. It can learn from examples of a “good” layout, where “good” may be defined by even non-differentiable metrics, e.g., edge crossings. While  $SGD^2$  and SmartGD are among the first graph embedding methods that can simultaneously optimize multiple criteria, neither works well beyond small graphs ( $|V| \approx 100$ ). The optimal projection algorithm proposed in this paper performs well on both small and large graphs (over 1000 nodes) while supporting multiple criteria.

While joint optimization seeks to be effective at minimizing a given metric while preserving the aesthetic appeal of the layout, it will not necessarily generate a drawing with any one criterion optimal. Of particular interest to the algorithmic community are algorithms that optimize a specific metric, possibly at the expense of readability.

One such algorithm is *Vertex Movement* [56] (VM), which optimizes edge crossings while ignoring other aesthetic criteria. The algorithm starts with an initial layout, iterates over the vertices, and tries to find the crossing-minimal position for the current vertex. While not guaranteed to find an optimal drawing, it achieves strong performance in finding drawings with few edge crossings. We use VM as a state-of-the-art baseline for crossing minimization, but note that this algorithm has high computational complexity, and cannot be applied to large graphs.

### 2.2 Understanding high-dimensional data through projection.

Paulovich et al. [53] recently linked dimensionality reduction and graph drawing, showing their close relationship. Algorithms and interactive systems for exploring high-dimensional data via projections have long

been studied, with early work in the statistics and physics communities [9, 13–15, 37, 45, 51]. Notable examples include the R-based visualization tool XGobi [9] and the Embedding Projector [58].

GraphDice [7] is a relevant tool for exploring and analyzing graph data. It supports exploration of multivariate social network graphs through animated transitions between nearby views. However, it operates on observed actor and edge attributes rather than on geometric projections of a high-dimensional graph embedding. EvoGraphDice [59] extends this line of work to general multidimensional data, using interactive evolutionary search to propose specific views based on user feedback. It is therefore relevant as a visual analytics approach to guided viewpoint discovery, but it is not designed for graph layouts or for optimizing graph-drawing metrics.

As far as we are aware, there is little prior work focused on understanding high-dimensional graph embeddings (beyond 2/3D) via optimal projection. Gajer et al. [25] demonstrated that laying out a graph in a high-dimensional space and randomly projecting it back to 2D can produce interesting drawings, illustrated using a Möbius strip example; however, their work does not aim to identify optimal views. Also related is work by Gaertler and Krug, who used animations between different viewpoints of a spectral graph embedding [24].

Li et al. [46] investigated methods for visualizing multidimensional data arising from neural networks. Although they examined nonlinear dimensionality reduction techniques such as t-SNE and UMAP, linear projections were favored due to their predictable response to changes in the original data. Etemadpour et al. [22] conducted a perception-based user study on multidimensional projections, showing that projection performance depends on tasks and data characteristics. The study shows that no single projection method yields universally optimal layouts, which supports the argument for generating and evaluating multiple views of high-dimensional graph layouts.

Martins et al. [48] introduce multidimensional projection methods for social network visualization, where node placement is guided by node similarity to produce meaningful 2D layouts without heavy force-based optimization. The work demonstrates that high-dimensional embeddings and projection-driven views can reveal structural patterns beyond conventional graph drawing, reinforcing the motivation for multi-view exploration of high-dimensional graph layouts.

It has been shown that 2D viewpoint drawings acquired from 3D drawings can be of higher quality than 2D drawings produced with the same algorithm [62]. This result is achieved through efficient optimization algorithms, including gradient descent and evolutionary-inspired metaheuristics, that automatically find high-quality viewpoints for 3D straight-line graph drawings, replacing slow brute-force sampling methods that require evaluating thousands of viewpoints. Although this viewpoint optimization is similar to the optimal projection found in DataFly, we aim to find good viewpoints for a K-D graph embedding instead. Recent findings [39] show that, after creating such a 3D drawing, users prefer to view it from angles that yield 2D projections with high values for several 2D quality metrics. Similar findings were shown for Dimensionality Reduction (DR) plots [10]. We primarily consider linear projections, though a rich set of non-linear DR techniques exist; see recent surveys [21, 52].

## 3 UNDERSTANDING GRAPHS THROUGH HIGH-DIMENSIONAL LAYOUTS

Here, we give a high level overview of our methodology. We use standard graph definitions:  $G = (V, E)$ , where  $V$  denotes the set of vertices and  $E$  denotes the set of edges. We posit that embedding graphs in a high-dimensional space enables a more faithful representation of their intrinsic structure, such as local neighborhoods. To this end, we first embed the graph in  $K$ -dimensional space (e.g.,  $K = 10$ ), using an off-the-shelf algorithm. What remains is to investigate potentially interesting 2D viewpoints of this embedding for visualization.

Figure 2 illustrates how different projections of the same 10D embedding can reveal qualitatively different structures. However, it is not clear that such viewpoints offer any real advantages for real-world data. We posit the following research questions:

**RQ1.** Do high-dimensional graph embeddings, when combined with carefully designed projection methods, offer advantages over direct 2D

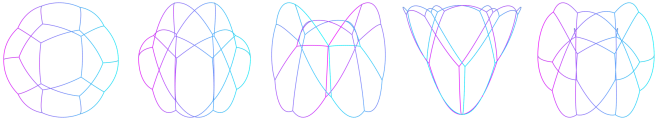


Fig. 2: Several projections of an 10D spectral embedding of a subdivided dodecahedron graph. The leftmost projection looks like a typical embedding, but other viewpoints reveal the structure twists and wraps on itself in the ambient space.

layouts in optimizing specific aesthetic metrics?

**RQ2.** Can exploring systematic projections of high-dimensional viewpoints help users understand graph structure?

We address **RQ1** through the optimal viewpoint formulations developed in this section and the quantitative evaluation in [Sec. 4](#). We address **RQ2** later through qualitative examples ([Sec. 4.3](#)) and by introducing an interactive tool, `DataFly`, evaluated through a usability study ([Sec. 6](#)).

In this section, we propose carefully designed 2D projections of high-dimensional layouts, referred to as *viewpoints*, to address **RQ1**. Our goal is to identify viewpoints that are most likely to provide informative insights into the graph structure.

### 3.1 High-dimensional layouts

Many graph layout algorithms generalize naturally to high dimensions. In our work we consider four approaches: a stress model [\[27\]](#), a force-directed algorithm [\[35\]](#), the spectral embedding algorithm [\[32\]](#), and PivotMDS [\[8\]](#). However, the pipeline we describe works for any embedding algorithm in principle.

For the stress model, we use `neato` [\[27\]](#) from the Graphviz library [\[30\]](#). Stress-based optimization is one of the standard 2D graph embedding methods and is available in most software platforms, ranging from Graphviz and NetworkX [\[31\]](#), to OGDF [\[12\]](#) and yFiles [\[66\]](#). Stress-based layouts are often included as a baseline when evaluating new methods, and the implementation in Graphviz is a trusted standard. The notion of stress ([Equation \(3\)](#)) is based on Euclidean distances and therefore well-defined in high dimensions. Human-subject studies [\[11, 50\]](#) have shown that lower stress is an important predictor of aesthetic preference in graph visualization.

Perhaps the only graph embedding methods as popular as stress-based models are force-directed methods [\[42\]](#). These methods typically minimize a spring-electrical energy ([Equation \(5\)](#)) that captures attractive forces between pairs of nodes connected by edges, and repulsive forces between all pairs of nodes. As a representative of force-directed algorithms, we use `sfdp` [\[35\]](#) from the Graphviz library [\[30\]](#). This is an efficient implementation frequently used as a baseline for evaluation.

We evaluate two additional algorithms as they naturally lay out graphs in up to  $|V|$  dimensions. The spectral algorithm [\[32\]](#) is based on taking the top  $K$ -eigenvectors of the Laplacian corresponding to the lowest  $K$ -eigenvalues. We use the implementation in the NetworkX library [\[31\]](#). We also include the PivotMDS algorithm [\[8\]](#), a scalable version of the classical MDS algorithm [\[60\]](#). It works by picking  $K$  pivot nodes, forming the squared and double-centered distance matrix to the pivots of dimension  $|V| \times K$ , and performing Principal Component Analysis (PCA) on this matrix. We re-implemented this based on the description in [\[8, 36\]](#).

Given the wide popularity of the stress metric, we present most of the results for projections of high-dimensional layouts produced by `neato`, alongside corresponding results for `sfdp`. Additional results are given in the Appendix. We also limit our evaluation to up to 10D embeddings, as GraphViz officially supports graph layouts in at most 10 dimensions.

Although higher dimensions provide more freedom for the layout to preserve connectivity, the final display of information to human readers is limited to the 2 dimensions of the computer screen. We must therefore rely on informative 2D projections to interpret these high-dimensional layouts.

### 3.2 Optimal Viewpoints

We define a *viewpoint* as a specific 2D projection of a  $K$ -D layout of a graph. While there are infinitely many possible viewpoints, some of them are more interesting than others.

An *optimal viewpoint* is defined as the projection from  $K$ -D to 2D that minimizes a specific metric  $\mathcal{L}$ . For brevity, we refer to locally optimized viewpoints as optimal viewpoints. We collectively call these viewpoint-optimizing algorithms `DataFly`.

Let  $X \in \mathbb{R}^{|V| \times K}$  denote a high-dimensional embedding matrix, where each row represents the  $K$ -D embedding of a node, obtained from an algorithm. The goal is then to learn a linear projection  $P \in \mathbb{R}^{K \times 2}$  that maps  $X$  to a two-dimensional space while minimizing a loss of the projected layout. Formally, we solve

$$\min_{P \in \mathbb{R}^{K \times 2}} \mathcal{L}(XP) \quad (1)$$

where  $\mathcal{L}$  is the graph metric, and  $XP \in \mathbb{R}^{|V| \times 2}$  gives the 2D coordinates resulting from the projection. Note that this optimization involves only  $2K$  variables (e.g.,  $K = 10$ ), which is far fewer than the  $2|V|$  variables that algorithms for traditional layouts must optimize over, making the problem easier and less computationally expensive to solve.

To find the optimal projection  $P$  in ([Equation \(1\)](#)), we use an iterative gradient descent algorithm, updated as:

$$P_{t+1} = P_t - \eta \nabla_{P_t} \mathcal{L}(XP_t), \quad (2)$$

where  $\eta$  is the step size.

### 3.3 Metrics

Graph layout quality is inherently multi-objective, and no single metric consistently captures aesthetic quality across different graphs and tasks. Different metrics instead reflect different, and sometimes competing, objectives—for example, stress emphasizes structural faithfulness, whereas edge crossings emphasize readability. Therefore, we explore a diverse set of complementary metrics to evaluate viewpoint quality. We denote  $x_i \in \mathbb{R}^d$  the coordinates of node  $i$  in  $d$  dimensions.

**Stress:** This metric measures the stress of the layout,

$$\text{stress} = \sum_{i,j \in V, i \neq j} w_{ij} (\alpha \|\mathbf{x}_i - \mathbf{x}_j\| - d_{ij})^2, \quad (3)$$

where  $d_{ij}$  is the desired distance between  $i$  and  $j$ , and  $w_{ij}$  is set to  $1/d_{ij}^2$ . Here, for a given layout, we apply a scaling factor of  $\alpha$  to normalize the stress (e.g., [\[57, 64\]](#)):

$$\alpha = \frac{\sum_{i,j \in V, i \neq j} w_{ij} d_{ij} \|\mathbf{x}_i - \mathbf{x}_j\|}{\sum_{i,j \in V, i \neq j} w_{ij} \|\mathbf{x}_i - \mathbf{x}_j\|^2}. \quad (4)$$

**Spring-Electrical Energy:** This metric treats edges as springs and nodes as electrically repelling particles and measures the energy of the system:

$$\text{se\_eng} = \sum_{(i,j) \in E} \frac{\|\mathbf{x}_i - \mathbf{x}_j\|^3}{3K_s} - \sum_{i \neq j} K_r \ln(\|\mathbf{x}_i - \mathbf{x}_j\|). \quad (5)$$

where  $K_s$  and  $K_r$  are spring and repulsion constants. We set them to 1. To make this metric scale-invariant, we use a scaling factor  $t$  that minimizes ([Equation \(5\)](#)). We derive an analytical solution (proof is given in the Appendix):  $t = \left( \frac{|V|(|V|-1)}{\sum_{(i,j) \in E} \|\mathbf{x}_i - \mathbf{x}_j\|^3} \right)^{1/3}$ .

**t-SNE Score:** This metric measures Kullback-Leibler divergence of node distances between the Euclidean layout space and the graph space using t-distributed stochastic neighbor embedding (t-SNE [\[47\]](#)). It evaluates how well the graph neighborhoods are preserved in the layout.

$$\text{tsne} = \sum_{\substack{i,j \\ i \neq j}} p_{ij} \log \frac{p_{ij}}{q_{ij}}, \quad (6)$$

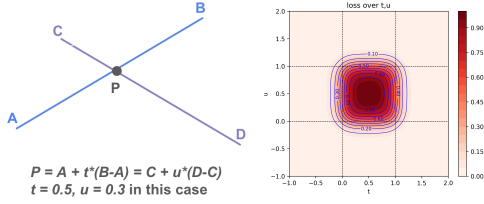


Fig. 3: Left: the edge-crossing parameters. Right: contour of the SigmoidX surrogate function for edge crossings.

where

$$p_{ij} = \frac{p_{j|i} + p_{i|j}}{2N}, p_{j|i} = \frac{\exp(-\frac{d_{ij}^2}{2\sigma_i^2})}{\sum_{k \neq i} \exp(-\frac{d_{ik}^2}{2\sigma_i^2})}, q_{ij} = \frac{(1 + \|\mathbf{x}_i - \mathbf{x}_j\|^2)^{-1}}{\sum_{k \neq l} (1 + \|\mathbf{x}_k - \mathbf{x}_l\|^2)^{-1}}$$

The t-SNE metric is not scale-invariant. When computing the optimal 2D projection, to ensure good initialization and a differentiable loss function, we normalize the coordinates using (Equation (4)). However, to ensure a fair comparison across methods, we rescale the coordinates for each layout using a 1-D minimization step before computing the reported metric.

**Edge crossings:** This metric counts the number of edge crossings in the layout, indicating visual clutter. Fewer crossings suggest a cleaner, more readable layout.

$$\text{xing} = \sum_{(i,j),(k,l) \in E, (i,j) \neq (k,l)} \mathbb{I}[\text{edge}(i,j) \text{ crosses } (k,l)]. \quad (7)$$

To apply gradient descent for minimizing edge crossing, a differentiable surrogate function is required. SGD<sup>2</sup> [1] learns a differentiable proxy for edge crossings by training a neural network to predict whether two edges intersect, based on their node coordinates. We instead propose a simpler approach. Let  $t, u$  be the intersection parameters in Figure 3 (left). Geometrically, when  $t \in [0, 1]$ , this means that the second edge, or its extension, hits the first edge. The parameter  $u$  is defined symmetrically to  $t$ . Hence, if the two edges cross, we must have that both  $t, u \in [0, 1]$ . But instead of using such a hard, non-differentiable condition to determine whether edges intersect, we use sigmoid-based soft masks:

$$M_t = \frac{\sigma(t) [1 - \sigma(t-1)]}{M_{\text{peak}}}, \quad M_u = \frac{\sigma(u) [1 - \sigma(u-1)]}{M_{\text{peak}}},$$

where  $\sigma(t) = \frac{1}{1+e^{-Tt}}$  is the sigmoid function, with temperature  $T$  controlling the steepness, and  $M_{\text{peak}}$  normalizing the peak value to 1.

The differentiable probability of an edge crossing is then  $P(\text{crossing}) = M_t M_u$ . It approaches 1 when the edges intersect ( $t, u \in [0, 1]$ ), but quickly and smoothly decreases toward 0 otherwise. We call this loss function *SigmoidX*. It is a continuous, differentiable proxy for the binary “edges intersect” test, enabling gradient-based minimization of edge crossings. We illustrate this function in Figure 3. Additional details are given in the Appendix Sec. A1. SigmoidX is used to find the optimal projection, but we report the actual edge crossings.

**Edge Length Variation:** This metric measures the standard deviation of all edge lengths. Let  $\ell_{ij} = \|\mathbf{x}_i - \mathbf{x}_j\|$  be the length of edge  $(i, j) \in E$ , then  $\text{edgelen\_var} = \text{std}(\ell_{ij}) / \text{mean}(\ell_{ij})$ . It captures uniformity in edge representation, affecting aesthetic clarity and interpretability.

**Angular Resolution:** This metric measures the minimum angle between incident edges at each node — higher resolution improves visual distinction and reduces ambiguity. Typically, it is defined as  $\pi - \min_{v \in V} \min_{\substack{(v,u), (v,w) \in E \\ u \neq w}} \arccos(\frac{\mathbf{x}_u - \mathbf{x}_v, \mathbf{x}_w - \mathbf{x}_v}{\|\mathbf{x}_u - \mathbf{x}_v\| \|\mathbf{x}_w - \mathbf{x}_v\|})$ . However, this

measure only focuses on the worst case, which has limited expressivity. In this paper, we aim to improve the angular resolution across all nodes; hence, we adopt an average measure of how evenly the neighbors of each node are distributed around it. For a node  $v$  with degree  $d_v \geq 2$ ,

the ideal angular spacing is  $\theta_v^* = \frac{2\pi}{d_v}$ . Let  $\hat{\theta}_v^{\min}$  be the smallest actual angle between consecutive neighbors of  $v$ . We define angular resolution as

$$\text{ang\_res} = \sqrt{\frac{1}{|V'|} \sum_{v \in V'} (\theta_v^* - \hat{\theta}_v^{\min})^2}, \quad (8)$$

where  $V' = \{v \mid d_v \geq 2\}$  is the set of nodes with degree over 1.

## 4 EXPERIMENTAL EVALUATION

To quantify the potential benefits of DataFly, we compare the metrics of baseline algorithms with those of the DataFly optimal viewpoints. Hereafter, we use `neato(K)` to denote the outcome of laying out a graph in K-D; the same notation applies to other algorithms. By default, `neato` refers to `neato(2)`. We denote  $\text{DF}_{\text{opt}}^{\text{neato}}(K)$  as the result of the DataFly optimal viewpoint on the `neato` K-D layout for a specific metric, and write  $\text{DF}_{\text{opt}}^{\text{neato}}$  for  $\text{DF}_{\text{opt}}^{\text{neato}}(10)$ . Similarly,  $\text{DF}_{\text{opt}}^{\text{sfdp}}$  denotes the optimal projection on the `sfdp` 10-D layout for a specific metric.

### 4.1 Experimental Setup

**Optimization procedure.** To find the optimal projection  $P$  in (Equation (1)), we initialize  $P$  using the first two principal components of the K-dimensional layout  $X$ . At each iteration  $t$ , we perform a gradient descent update (Equation (2)) with a learning rate of  $\eta = 0.1$ , using the Adam [41] optimizer. The algorithm tracks the best projection matrix  $P$  and the corresponding projected coordinates  $XP$  that yield the lowest metric value observed during training. We run up to 200 epochs, which we found sufficient for convergence in most cases.

Across multiple runs, we found that  $\text{DF}_{\text{opt}}^{\text{neato}}$  and  $\text{DF}_{\text{opt}}^{\text{sfdp}}$  produced stable results, likely due to the deterministic initialization of  $P$ . The GraphViz implementations of `neato` and `sfdp` are known to be stable, and provide consistent results.

**Benchmark Datasets.** We evaluate using two benchmark datasets. SuiteSparse14 consists of 14 test graphs chosen from the SuiteSparse matrix collection [16]. They are selected to include graphs of different types (e.g., originating from structural, power network, and scientific problems). The two exceptions are “mobius”, which is generated from a  $5 \times 50$  mesh graph of a Möbius strip. This graph was used as an example in Gajer et al. [25] to motivate the need for high-dimensional layouts of graphs. We also include the  $2^{10}$ -dimensional hypercube “hypercube10”, since it can only be realized without distortion in 10D. The number of nodes and edges is shown in the first column of Tab. 1, under the name of each graph. For disconnected graphs, the largest component is taken.

The second benchmark is the Rome graph collection [3], comprising 11,531 relatively sparse graphs with 10–100 vertices and 9–158 edges. We include this dataset to enable comparison with metric-optimizing baseline algorithms SGD<sup>2</sup> [1] and SmartGD [64], which were originally designed for smaller graphs and therefore require a small-graph benchmark. To present results here, we randomly selected 20 graphs from the benchmark for illustration purposes, which we refer to as Rome20.

**Aggregating performance metrics.** To summarize the comparison between DataFly and other algorithms over many graphs, we report the SPC metric [63], defined as the average relative difference between the metrics of DataFly and the baseline, over the test graphs. *Smaller values are better.* For example, when comparing algorithm A with the baseline algorithm B, a SPC =  $-0.05$  indicates that A is on average 5% better than B under that metric. Specifically,

$$\text{SPC} = \frac{1}{m} \sum_{i=1}^m \frac{A_i - B_i}{\max(|A_i|, |B_i|)}, \quad (9)$$

where  $A_i$  and  $B_i$  denote the metrics for the algorithm of interest and the baseline algorithm, for test graph  $i$ , and  $m$  is the number of test graphs.

### 4.2 Comparing DataFly with Baseline Algorithms

Traditional graph layout algorithms, such as force-directed methods and stress majorization [20, 23, 26], optimize functions directly in low-dimensional spaces (e.g., 2D or 3D), where they are more likely to get

trapped in local minima. In contrast, optimizing the same problem in higher dimensions offers more degrees of freedom, helping escape local minima that often become saddle points in higher dimensions, which still admit descent directions [28] (Section 8.2.3). Given this, a natural question arises: can DataFly achieve lower stress than *neato*, lower spring-electrical energy than *sfdp*, and improvements across other layout quality metrics?

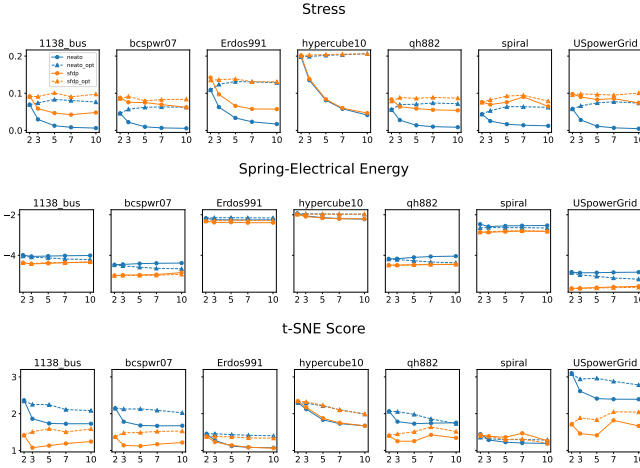


Fig. 4: Example curves showing how metrics change when *neato* and *sfdp* are embedded in higher dimensions: solid lines show values in the ambient dimension, and dotted lines show values after optimal projection. Stress improves markedly with added dimensions, but this also makes low-stress projections harder to obtain. Spring-electrical energy gains little from extra dimensions. For the t-SNE score, higher dimensions often increase the metric, while projecting down from them typically outperforms direct 2D optimization.

**Comparison with *neato*.** Results are summarized in Tab. 1. We first note that, as embedding dimensions increase, it is intuitively much easier for the Euclidean distance in the layout to approximate the graph-theoretic distance, resulting in lower stress (Equation (3)). As shown in Figure 4 and Tab. A3 in the Appendix, the stress decreases as the ambient dimension increases. Stress in 10-D is 84.4% lower on average than in 2D.

However, does this lower stress in high dimensions result in DataFly achieving lower stress than a 2D optimized *neato*? As shown in Tab. 1 (left), this can be true in some cases, e.g., for “Si2”,  $DF_{opt}^{neato}$  achieved a stress of 0.143 vs 0.159 for *neato*. Overall, the SPC aggregate metric shows that stress for  $DF_{opt}^{neato}$  is 12.2% higher (worse) than for *neato*. This suggests that while *neato* can occasionally get trapped in a local optimum in 2D, this is infrequent — *neato* generally achieves lower stress in 2D.

When considering other metrics, the advantage of DataFly becomes clearer.  $DF_{opt}^{neato}$  achieves 12.8% better angular resolution, 16.9% lower edge-length variance, 7.44% better t-SNE score, and 23.3% fewer edge crossings. Its performance on spring-electrical energy is on par with direct *neato* 2D layouts.

Figure A1 (top) in the Appendix shows paired-bootstrap ( $n = 5000$ ) 95% confidence intervals (CIs) for the SPC metric across evaluation measures. A CI entirely below 0 indicates  $DF_{opt}^{neato}$  significantly outperforms *neato*. Under this view,  $DF_{opt}^{neato}$  clearly outperforms in angular resolution, edge length variance, t-SNE score, and edge crossings. SPC values for these metrics in Tab. 1 are marked with \*, and the same convention is used for subsequent results.

**Comparison with *sfdp*.** The spring-electrical energy, which *sfdp* optimizes, decreases as the layout dimension increases, as shown in Figure 4 and Tab. A5 in the Appendix. However, the reduction is not as drastic as we saw with stress and *neato* (Tab. A3). Overall, spring-electrical energy is 10.6% lower in 10-D than in 2D. In particular, when the graphs originate from 2D applications (e.g., 1138\_bus and USpowerGrid), higher dimensions do not help at all, while for other graphs (e.g., email, EX1), higher dimensions improve spring-electrical

energy, though not significantly. This seems to indicate that an optimal layout for this loss function can be realized well in a lower dimension. One way to assess whether a high-dimensional embedding can “live” comfortably in a lower-dimensional subspace is to examine the variance explained by PCA [34] when projecting to that lower dimension. The results in the Appendix (Tab. A6) support this: at the same target dimension, the PCA-explained variance for *sfdp* is consistently higher than for *neato*. For example, projecting 10D embeddings to 2D via PCA retains 75.4% of the original variance for *sfdp*, compared with 70.2% for *neato*.

The optimal projection  $DF_{opt}^{sfdp}$  achieves similar (within 2%) spring-electrical energy, stress, and t-SNE score as *sfdp*; see Tab. 1 (right).

However,  $DF_{opt}^{sfdp}$  performs better on angular resolution, edge length variance, and edge crossings.

	<i>neato</i>	ang_res↓	edge_len↓	spr_elec↓	stress↓	t-SNE↓	xing↓
1138_bus		1.171, 1.154	<b>0.296</b> , 0.409	-3.988, -4.212	<b>0.069</b> , 0.076	2.365, <b>2.085</b>	1406, <b>1199</b>
bcsprw07		1.16, <b>1.096</b>	<b>0.291</b> , 0.402	-4.465, -4.664	<b>0.046</b> , 0.062	2.149, <b>2.024</b>	1572, <b>1570</b>
email		1.191, <b>0.996</b>	<b>0.515</b> , 0.477	-2.151, -2.114	<b>0.133</b> , 0.163	1.369, <b>1.336</b>	544390, <b>517851</b>
Erdos991		1.277, <b>1.132</b>	<b>0.439</b> , 0.409	-2.117, -2.157	<b>0.109</b> , 0.129	1.451, <b>1.398</b>	35664, <b>29064</b>
EX1		0.39, <b>0.374</b>	<b>0.339</b> , 0.201	-1.458, -1.477	<b>0.167</b> , 0.176	1.153, <b>1.123</b>	487248, <b>340132</b>
football		0.541, <b>0.529</b>	<b>0.424</b> , 0.399	-1.167, -1.17	<b>0.128</b> , 0.132	0.539, <b>0.518</b>	6843, <b>5183</b>
hypercube10		0.595, <b>0.323</b>	<b>0.341</b> , 0.007	-1.935, -1.972	<b>0.198</b> , 0.206	2.302, <b>1.987</b>	478232, <b>247989</b>
Journals		0.077, <b>0.075</b>	<b>0.434</b> , 0.463	0.21, 0.243	<b>0.167</b> , 0.182	0.079, <b>0.077</b>	3747293, <b>3156318</b>
mobius		0.639, <b>0.464</b>	<b>0.187</b> , 0.089	-3.535, -3.603	<b>0.029</b> , 0.034	0.759, <b>0.735</b>	72, <b>37</b>
qh882		1.277, <b>1.237</b>	<b>0.421</b> , 0.323	-1.177, -1.369	<b>0.056</b> , 0.072	2.065, <b>1.73</b>	7590, <b>5361</b>
Si2		0.317, <b>0.308</b>	<b>0.536</b> , 0.384	-1.421, -1.555	<b>0.159</b> , 0.143	0.907, <b>0.828</b>	1745046, <b>1150696</b>
spiral		0.533, <b>0.283</b>	<b>0.467</b> , 0.44	-2.464, -2.653	<b>0.044</b> , 0.062	1.443, <b>1.284</b>	853028, <b>638663</b>
Trefethen_700		0.353, <b>0.346</b>	<b>0.616</b> , 0.341	-1.481, -1.498	<b>0.177</b> , 0.181	1.209, <b>1.103</b>	667259, <b>457958</b>
USpowerGrid		1.246, <b>1.156</b>	<b>0.372</b> , 0.438	-4.829, -5.177	<b>0.058</b> , 0.073	3.1, <b>2.782</b>	12364, <b>12273</b>

Fig. 5: Optimal projections of the 10D *neato* layout. Numbers represent (*neato*,  $DF_{opt}^{neato}$ ) metrics. **Bold** = better. Edges colored by length: red = short, blue = long.

### 4.3 Visualizations with DataFly

It is informative to compare the optimal projection viewpoints identified by DataFly with those obtained from the corresponding baseline algorithms. Figure 5 presents visualizations from  $DF_{opt}^{neato}$  alongside those from *neato*. DataFly sometimes reveals compelling graph structures that differ markedly from those produced by *neato*. For example, for the “Si2” and “EX1” graphs, the DataFly visualization that optimizes edge crossings highlights a lattice structure that is less apparent in the *neato* layout. Similarly, for “mobius”, the DataFly viewpoint that minimizes edge crossings is much smoother and has half as many edge crossings as *neato* (37 vs. 72). In “Trefethen\_700”, DataFly produces a clearer, more organized layout that reveals lin-

Table 1: Comparison of metrics on SuiteSparse14 for two method pairs: `neato` (2D) vs.  $DF_{opt}^{neato}$  and `sfdp` (2D) vs.  $DF_{opt}^{sfdp}$ . Lower is better for all metrics. The best value within each method pair and graph/metric combination is highlighted in bold. The number of nodes/edges is shown in parentheses under the graph names. SPC values marked with \* are statistically significant (Appendix Figure A1).

Graph	mthd	neato vs. $DF_{opt}^{neato}$					xing↓	mthd	sfdp vs. $DF_{opt}^{sfdp}$					xing↓
		ang_r↓	edglen↓	spr_el↓	stress↓	t-SNE↓			ang_r↓	edglen↓	spr_el↓	stress↓	t-SNE↓	
1138_bus (1138,1458)	<code>neato</code>	1.173	<b>0.296</b>	-3.988	<b>0.069</b>	2.365	1406	<code>sfdp</code>	<b>1.046</b>	<b>0.550</b>	<b>-4.369</b>	<b>0.092</b>	<b>1.415</b>	<b>511</b>
	$DF_{opt}^{neato}$	<b>1.154</b>	0.409	<b>-4.212</b>	0.076	<b>2.085</b>	<b>1199</b>	$DF_{opt}^{sfdp}$	1.105	0.569	-4.322	0.098	1.584	756
bcspwr07 (1612,2106)	<code>neato</code>	1.160	<b>0.291</b>	-4.465	<b>0.046</b>	2.149	1572	<code>sfdp</code>	1.033	0.672	<b>-4.998</b>	0.088	<b>1.365</b>	<b>678</b>
	$DF_{opt}^{neato}$	<b>1.096</b>	0.402	<b>-4.664</b>	0.062	<b>2.024</b>	<b>1570</b>	$DF_{opt}^{sfdp}$	<b>1.030</b>	<b>0.568</b>	-4.937	<b>0.084</b>	1.526	814
email (1133,5451)	<code>neato</code>	1.191	0.515	<b>-2.151</b>	<b>0.133</b>	1.369	54490	<code>sfdp</code>	1.207	0.546	<b>-2.306</b>	<b>0.142</b>	<b>1.308</b>	425417
	$DF_{opt}^{neato}$	<b>0.996</b>	<b>0.477</b>	-2.114	0.163	<b>1.336</b>	<b>517851</b>	$DF_{opt}^{sfdp}$	<b>1.097</b>	<b>0.529</b>	-2.269	0.150	1.309	<b>399532</b>
Erdos991 (446,1413)	<code>neato</code>	1.277	0.439	<b>-2.170</b>	<b>0.109</b>	1.451	35664	<code>sfdp</code>	1.260	0.502	<b>-2.313</b>	0.142	1.378	32632
	$DF_{opt}^{neato}$	<b>1.132</b>	<b>0.409</b>	-2.157	0.129	<b>1.398</b>	<b>29064</b>	$DF_{opt}^{sfdp}$	<b>1.183</b>	<b>0.465</b>	-2.280	<b>0.131</b>	<b>1.334</b>	<b>27855</b>
EX1 (560,4368)	<code>neato</code>	0.390	0.339	-1.458	<b>0.167</b>	1.153	487248	<code>sfdp</code>	0.390	0.205	<b>-1.493</b>	<b>0.170</b>	1.167	492441
	$DF_{opt}^{neato}$	<b>0.374</b>	<b>0.201</b>	<b>-1.477</b>	0.176	<b>1.123</b>	<b>340132</b>	$DF_{opt}^{sfdp}$	<b>0.367</b>	<b>0.183</b>	-1.486	0.175	<b>1.089</b>	<b>364237</b>
football (115,613)	<code>neato</code>	0.541	0.424	-1.167	<b>0.128</b>	0.539	6843	<code>sfdp</code>	0.539	0.519	<b>-1.196</b>	0.138	0.508	5622
	$DF_{opt}^{neato}$	<b>0.529</b>	<b>0.399</b>	<b>-1.170</b>	0.132	<b>0.518</b>	<b>5183</b>	$DF_{opt}^{sfdp}$	<b>0.526</b>	<b>0.438</b>	-1.181	<b>0.135</b>	<b>0.507</b>	<b>5334</b>
hypercube10 (1024,5120)	<code>neato</code>	0.595	0.341	-1.935	<b>0.198</b>	2.302	478232	<code>sfdp</code>	0.486	0.081	<b>-1.980</b>	<b>0.202</b>	2.343	518024
	$DF_{opt}^{neato}$	<b>0.323</b>	<b>0.007</b>	<b>-1.972</b>	0.206	<b>1.987</b>	<b>247989</b>	$DF_{opt}^{sfdp}$	<b>0.356</b>	<b>0.040</b>	-1.970	0.206	<b>1.991</b>	<b>264487</b>
Journals (124,5972)	<code>neato</code>	0.077	<b>0.434</b>	<b>0.210</b>	<b>0.167</b>	0.079	3747293	<code>sfdp</code>	0.077	<b>0.446</b>	<b>0.210</b>	<b>0.170</b>	0.078	<b>3720645</b>
	$DF_{opt}^{neato}$	<b>0.075</b>	0.463	0.243	0.182	<b>0.077</b>	<b>3156318</b>	$DF_{opt}^{sfdp}$	<b>0.074</b>	0.462	0.237	0.182	<b>0.077</b>	3741769
mobius (250,450)	<code>neato</code>	0.639	0.187	-3.535	<b>0.029</b>	0.759	72	<code>sfdp</code>	0.819	0.524	<b>-3.607</b>	0.038	0.812	37
	$DF_{opt}^{neato}$	<b>0.464</b>	<b>0.089</b>	<b>-3.603</b>	0.034	<b>0.735</b>	<b>37</b>	$DF_{opt}^{sfdp}$	<b>0.650</b>	<b>0.193</b>	-3.592	0.038	<b>0.730</b>	<b>14</b>
qh882 (1764,3354)	<code>neato</code>	1.277	0.421	-4.177	<b>0.056</b>	2.065	7590	<code>sfdp</code>	<b>1.311</b>	0.874	<b>-4.484</b>	<b>0.083</b>	<b>1.399</b>	<b>4337</b>
	$DF_{opt}^{neato}$	<b>1.237</b>	<b>0.323</b>	<b>-4.369</b>	0.072	<b>1.730</b>	<b>5361</b>	$DF_{opt}^{sfdp}$	1.356	<b>0.752</b>	-4.442	0.087	1.515	5283
Si2 (769,8516)	<code>neato</code>	0.317	0.536	-1.421	0.159	0.907	1745046	<code>sfdp</code>	0.326	0.569	<b>-1.568</b>	<b>0.141</b>	<b>0.825</b>	1242149
	$DF_{opt}^{neato}$	<b>0.308</b>	<b>0.384</b>	<b>-1.555</b>	<b>0.143</b>	<b>0.828</b>	<b>1150696</b>	$DF_{opt}^{sfdp}$	<b>0.307</b>	<b>0.393</b>	-1.561	0.146	0.830	<b>1229816</b>
spiral (665,7657)	<code>neato</code>	0.533	0.467	-2.464	<b>0.044</b>	1.443	853028	<code>sfdp</code>	0.349	0.685	<b>-2.857</b>	<b>0.076</b>	1.424	725528
	$DF_{opt}^{neato}$	<b>0.283</b>	<b>0.440</b>	<b>-2.653</b>	0.062	<b>1.284</b>	<b>638663</b>	$DF_{opt}^{sfdp}$	<b>0.340</b>	<b>0.618</b>	-2.815	0.079	<b>1.193</b>	<b>689046</b>
Trefethen (700,5977)	<code>neato</code>	0.353	0.616	-1.481	<b>0.177</b>	1.209	667259	<code>sfdp</code>	0.352	0.519	<b>-1.512</b>	0.180	1.239	696237
	$DF_{opt}^{neato}$	<b>0.346</b>	<b>0.341</b>	<b>-1.498</b>	0.181	<b>1.103</b>	<b>457958</b>	$DF_{opt}^{sfdp}$	<b>0.348</b>	<b>0.348</b>	-1.503	<b>0.179</b>	<b>1.132</b>	<b>519729</b>
USpower (4941,6594)	<code>neato</code>	1.246	<b>0.372</b>	-4.829	<b>0.058</b>	3.100	12364	<code>sfdp</code>	<b>1.066</b>	0.795	<b>-5.633</b>	<b>0.098</b>	<b>1.712</b>	<b>3614</b>
	$DF_{opt}^{neato}$	<b>1.156</b>	0.438	<b>-5.177</b>	0.073	<b>2.782</b>	<b>12273</b>	$DF_{opt}^{sfdp}$	1.129	<b>0.773</b>	-5.579	0.101	2.044	5207
SPC↓		<b>-0.128*</b>	<b>-0.169*</b>	<b>-0.019</b>	0.122*	<b>-0.0744*</b>	<b>-0.233*</b>		<b>-0.050*</b>	<b>-0.178*</b>	0.017*	0.015	<b>-0.011</b>	<b>-0.068</b>

ear and rectangular patterns, while the `neato` layout appears more entangled, with increased edge crossings and visual clutter. Additional visual comparisons between `neato`, `sfdp`, and `DataFly` are given in the Appendix (Tabs. A1 and A2 and Tab. A4), which further confirm the effectiveness of `DataFly` in revealing graph structures that may be obscured in direct 2D layouts. These findings provide strong support for RQ1.

#### 4.4 Comparing DataFly with Other Algorithms

We observe that embedding graphs into high dimensions and then finding the optimal 2D projection can produce layouts with substantially better metric scores than those generated by baseline 2D algorithms (e.g., `neato` or `sfdp`). To understand how effective this approach is compared with directly optimizing the metrics, we compare `DataFly` with `SGD2` [1] and `SmartGD` [64] in minimizing edge crossings, and with `SGD2` on angular resolution and edge length variance. We were unable to obtain comparable results for `SGD2` and `SmartGD` across other metrics from the authors of these algorithms.

`SGD2` is designed to optimize several graph aesthetic metrics directly using gradient descent on relatively small graphs. `SmartGD` was also trained on the Rome collection of small graphs to optimize specific metrics using a generative adversarial network [38]. Therefore, we first used the Rome20 dataset for comparison.

The results are given in Tab. 2, with CIs analyzed in the Appendix Figure A2. For minimizing edge crossings, the last row of the table shows that  $DF_{opt}^{neato}$  achieves 22.1% fewer crossings on average than `SGD2`, while `SmartGD` is 4.4% better than `SGD2`. In terms of CPU time,  $DF_{opt}^{neato}$  took only 10 seconds, `SmartGD` takes 1 second, while the `SGD2` algorithm took over 1280 seconds. This also indicates that the gradient for crossing minimization in `SGD2`, which involves a neural network model that approximates the crossings, requires significant

computational effort. The best performing algorithm, Vertex Movement (VM) [56], takes 760 seconds and is 60.3% better than `SGD2`. While VM achieves low crossing numbers, it produces drawings that do not optimize other aesthetic criteria; see the example drawing of `grafo7023` in Figure A4, versus the corresponding drawing produced by `DataFly` in Tab. A2 (row 5, last column).

In terms of angular resolution,  $DF_{opt}^{neato}$  is 62% better than `SGD2` and again much faster, requiring only a few seconds vs 218 seconds for `SGD2`. When looking at edge length variance, `SGD2` reduced it to almost zero and performed better than `DataFly`. This is not a surprise, since even though edge length variance should be very low in high dimensions, linear projection is unlikely to preserve it due to the different orientations of edges in high dimensions. However, `SGD2` required 148 seconds, while  $DF_{opt}^{neato}$  completed in 10 seconds.

#### 4.5 Additional comparison on edge crossing minimization

As seen in Tab. 1, edge-crossings for both  $DF_{opt}^{sfdp}$  and `sfdp` are generally lower than for `neato` and  $DF_{opt}^{neato}$ . We formally compare these four algorithms together with `SmartGD` and `SGD2` on crossing minimization of the SuiteSparse14 dataset in Tab. 3. Indeed, on average, `sfdp` has 25.9% fewer crossings than `neato`, while  $DF_{opt}^{sfdp}$  has 33.9% fewer crossings. This is surprising given that in the graph drawing community, minimizing stress (which `neato` does) and minimizing crossings were known to be highly associated with user preference [19, 54].

We observe that `SmartGD` and `SGD2` have substantially higher edge crossings (70% and 54.5% worse than `neato`), while the two `DataFly` algorithms achieve improvements of 23.3% and 35% over `neato`. This confirms that neither `SmartGD` nor `SGD2` works well for large graphs. Comparing the runtime on these large graphs,  $DF_{opt}^{neato}$  and  $DF_{opt}^{sfdp}$  take 10,470 and 9,800 seconds, respectively. `SGD2` is the slow-

Table 2: Comparison on Rome20 graphs. We used SGD<sup>2</sup> as the benchmark. \* = statistically significant (Appendix Figure A2).

grafo id	xing↓			VM	ang_res↓		edge_len↓	
	DF <sup>neato</sup> <sub>opt</sub>	SGD <sup>2</sup>	SmartGD		DF <sup>neato</sup> <sub>opt</sub>	SGD <sup>2</sup>	DF <sup>neato</sup> <sub>opt</sub>	SGD <sup>2</sup>
2815.35	2	8	2	1	<b>0.700</b>	2.158	0.097	<b>0.012</b>
10379.95	82	80	82	40	<b>0.773</b>	1.881	<b>0.282</b>	0.388
9033.80	54	54	49	30	<b>0.778</b>	1.681	<b>0.279</b>	0.306
11674.33	3	5	6	1	<b>0.615</b>	1.997	0.122	<b>0.000</b>
847.22	4	16	5	0	<b>0.622</b>	1.808	0.051	<b>0.000</b>
762.27	3	5	3	1	<b>0.568</b>	1.980	0.157	<b>0.000</b>
11412.32	1	0	1	0	<b>0.696</b>	2.171	0.116	<b>0.000</b>
1583.66	12	18	15	9	<b>0.704</b>	2.085	0.245	<b>0.206</b>
3587.36	7	8	7	3	<b>0.868</b>	1.848	0.173	<b>0.013</b>
8296.86	66	50	79	42	<b>0.771</b>	1.798	<b>0.240</b>	0.302
11543.34	0	7	4	0	<b>0.753</b>	2.114	0.174	<b>0.021</b>
7023.45	8	16	12	2	<b>0.718</b>	2.034	0.194	<b>0.095</b>
9592.72	13	24	18	3	<b>0.692</b>	2.102	0.204	<b>0.174</b>
3138.60	31	18	42	20	<b>0.889</b>	2.161	<b>0.226</b>	0.294
2955.38	6	10	16	5	<b>0.754</b>	1.968	0.217	<b>0.039</b>
10480.95	59	81	63	30	<b>0.835</b>	1.934	<b>0.296</b>	0.307
2747.16	0	0	0	0	<b>0.635</b>	2.038	0.046	<b>0.000</b>
5780.48	25	30	33	13	<b>0.886</b>	1.703	0.203	<b>0.102</b>
11311.40	4	12	6	5	<b>0.696</b>	2.097	0.216	<b>0.143</b>
10451.95	96	64	116	50	<b>0.868</b>	1.805	<b>0.278</b>	0.337
SPC	-0.221*	0	-0.044	<b>-0.603*</b>	<b>-0.620*</b>		0	<b>0.456*</b>

Table 3: Comparing edge-crossings for various algorithms on SuiteSparse14. \* = statistically significant (Appendix Figure A3)

	neato	DF <sup>neato</sup> <sub>opt</sub>	sfdp	DF <sup>sfdp</sup> <sub>opt</sub>	SmartGD	SGD <sup>2</sup>
1138_bus	1406	1199	<b>511</b>	756	12061	15431
bcsfwr07	1572	1570	<b>678</b>	814	22176	47795
email	544390	517851	425417	<b>399532</b>	2852817	1234370
Erdos991	35664	29064	32632	<b>27855</b>	138411	47165
EX1	487248	<b>340132</b>	492441	364237	1862924	741591
football	6843	<b>5183</b>	5622	5334	9353	5578
hypercube10	478232	<b>247989</b>	518024	264487	2821132	1111129
Journals	3747293	3156318	3720645	3741769	3607080	<b>2772694</b>
mobius	72	37	37	<b>14</b>	10704	544
qh882	7590	5361	<b>4337</b>	5283	47892	203344
Si2	1745046	<b>1150696</b>	1242149	1229816	4181606	3347111
spiral	853028	<b>638663</b>	725528	689046	2338855	2006179
Trefethen	667259	<b>457958</b>	696237	519729	1878613	1723377
USpower	12364	12273	<b>3614</b>	5207	201292	1254507
SPC	0	-0.233*	-0.259*	<b>-0.339*</b>	0.700*	0.545*

est, taking 16,500 seconds. DF<sup>neato</sup><sub>opt</sub> and DF<sup>sfdp</sup><sub>opt</sub> are only moderately faster because, although their optimization involves only 20 variables, compared with 2|V| variables for SGD<sup>2</sup>, that advantage is offset by the high cost of computing the edge-crossings loss required for these algorithms. Inference with SmartGD is fast on these large graphs, taking only 315 seconds, reflecting its neural network-based, non-iterative nature; however, training the model demands substantial data and computational resources.

We also ran the edge-crossing minimization algorithm *Vertex Movement* (VM) [56] on these large graphs, but it did not finish within 24 hours for 9 of the 14 instances, confirming its scalability limitations.

Finally, for a comprehensive evaluation of edge-crossing minimization on small graphs, we compared all the algorithms on the complete Rome graph collection in Tab. 4. On this full set of 11,531

Table 4: SPC for edge crossings relative to neato over all Rome Graphs. \* = statistically significant (Appendix Figure A3)

	neato	DF <sup>neato</sup> <sub>opt</sub>	sfdp	DF <sup>sfdp</sup> <sub>opt</sub>	SmartGD	SGD <sup>2</sup>
SPC	0	<b>-0.268*</b>	-0.0338*	-0.215*	-0.0393*	-0.0477*

graphs, DF<sup>neato</sup><sub>opt</sub> and DF<sup>sfdp</sup><sub>opt</sub> have 26.8% and 21.5% lower edge crossings than neato, respectively. Both substantially outperform SGD<sup>2</sup> and SmartGD, although the latter two do surpass neato. Regarding the runtime, DF<sup>neato</sup><sub>opt</sub> and DF<sup>sfdp</sup><sub>opt</sub> each take about 3300 seconds for all graphs. The inference of SmartGD is also very fast on these small graphs, taking just 615 seconds. The geometric heuristic VM is slower, taking 122,000 seconds; furthermore, *it failed on 12% of the graphs due to floating-point errors*. Therefore, we do not include VM in the table. SGD<sup>2</sup> is the slowest, requiring 558,000 seconds, almost 170 times longer than DF<sup>neato</sup><sub>opt</sub> and DF<sup>sfdp</sup><sub>opt</sub>.

#### 4.6 Findings for RQ1

When comparing DataFly with the two baseline algorithms neato and sfdp across eight different evaluation metrics, DataFly outperformed them on six metrics. When comparing it with the two state-of-the-art algorithms SmartGD and SGD<sup>2</sup>, which are designed to optimize specific metrics, we found that DataFly is highly effective at minimizing edge crossings and improving angular resolution. While VM achieves the absolute lowest number of edge crossings, it is designed solely for that objective and has very high computational complexity. VM does not produce an aesthetic layout and is not suitable for large graphs. These observations support an affirmative answer to RQ1.

### 5 DATAFLY EXPLORATION TOOL

The DataFly application is a web-based platform for interactively exploring high-dimensional graph embeddings through different viewpoints. Having established that these viewpoints are quantitatively strong (Sec. 4) and qualitatively informative (Figure 5), we now describe the system that exposes them to users. Through interactive 2D visualizations, DataFly reveals patterns and structures that may be hidden in a static layout by allowing users to navigate among related projections. In addition to optimal projections, DataFly supports PCA projections, which are particularly well-suited for interactive exploration. We describe the PCA projections next, then the system’s main functionality, and finally a usability study.

#### 5.1 PCA viewpoints and interactive rotation

Given the  $K$ -dimensional node-embeddings matrix  $X \in \mathbb{R}^{|V| \times K}$ , we compute its principal components through Principal Component Analysis (PCA) [34]. PCA yields  $K$  orthogonal directions in the embedding space, ranked by decreasing variance of the projected points, that is, the spread of nodes in the projection. The first principal component captures the most variance, the second the next most, and so on. Any pair of principal components can be used as the axes of a 2D projection, yielding up to  $\binom{K}{2} = K(K-1)/2$  possible 2D viewpoints. In the tool, these viewpoints provide a structured set of interpretable linear projections that users can browse interactively.

To support informed exploration, we compute quality metrics such as stress and edge crossings for each candidate viewpoint and display them as a line chart at the bottom of the UI (Figure 6). The user can then navigate to the view that optimizes a given metric by clicking either the corresponding point on the line chart or its thumbnail. Since computing these metrics for every possible viewpoint is expensive, we first rank all principal-component pairs by their explained variance and retain only the top 50. Beyond the practical limitation that the interface can display only a limited number of viewpoints along the  $x$ -axis, this filtering is motivated by the observation that low-variance projections tend to cluster nodes tightly, leading to visual occlusion. Empirically, the most insightful views typically correspond to component pairs that capture relatively high variance (i.e., greater spatial spread).

#### 5.2 User Interface and Functionality

Figure 6 shows the DataFly visualization and interactive exploration system, with components labeled in the figure (e.g.,  $\textcircled{A}$ ). Users begin by uploading a file or selecting a built-in demo dataset  $\textcircled{A}$ . The system processes the data and renders the visualization  $\textcircled{B}$ . Users can configure the layout algorithm (neato, sfdp, PivotMDS, or spectral), the

initial embedding dimension (2–10), and the projection method (PCA or optimal projection) via ⑥.

By default, edges are colored according to a breadth-first traversal of the graph. The coloring is intended as a stable visual anchor (rather than a semantic encoding of graph properties) that helps preserve the user’s mental map as the visualization “flies” from one viewpoint to another. Nodes can also be highlighted to further support mental map preservation. Mouse-based zooming, panning are supported and instructed in a translucent information panel ⑧.

**Interaction modes.** Three modes are provided. The first is the *optimal-projection* mode: when the “Projection Algorithm” in ⑥ is set to “optimal projection,” DataFly presents the layout that optimizes stress as the main display ④ (depicted inset in the figure for demonstration), along with six thumbnails ⑦ corresponding to optimal projections for stress, edge crossings, t-SNE, spring-electrical energy, angular resolution, and edge-length variation, respectively. The value achieved by each of the six layouts for the currently selected metric is displayed above the thumbnails ⑦ in the optimal projection interface ④.

The PCA mode displays thumbnails ③ as previews of 2D projections from PCA component pairs sorted by the selected metric (default: highest to lowest variance). The toggle list in ⑤ supports re-sorting by a different metric. Users can browse thumbnails to spot patterns and click to transition to the selected viewpoint. The “Projection” sliders in ⑩ let users manually select PC combinations, triggering a transition animation. From the panel ⑨, users can view projection details, bookmark rotated projections, and quickly switch to saved views.

Thirdly, the system also provides an automatic cinematic mode, allowing users to initiate transition animations through all viewpoints by clicking the “DataFly” button ①, and to pause or resume at any time by pressing the space key.

**Interactive rotation.** Users can drag the view to perform a local rotation within a 3D exploration subspace. For PCA projections, this subspace is spanned by the two principal components of the current viewpoint and the remaining component with the highest variance; in optimal projection mode, it is formed by the optimized projection plane and an additional orthogonal direction. In both cases, the resulting viewpoint remains a linear projection, preserving interpretability while letting users perturb a view, extract structure from motion, mitigate node occlusion, and inspect nearby projections without losing continuity.

Together, these functionalities and interface elements are intended to support three complementary tasks: overview, selection, and refinement. Thumbnails ③ and ⑦ provide an overview of all viewpoints at once, and users can switch easily to a projection by clicking on a thumbnail; the line chart section ⑥ supports quantitative comparison by quality metrics and selection of views that optimize a chosen criterion; and direct interactions (e.g., zooming, panning, interactive rotation) support local refinement near a promising view. Animated transitions and a consistent edge-coloring scheme, together with node highlighting, help preserve correspondence between successive projections, so users can compare related views as transformations of the same embedding rather than as unrelated layouts.

**Scalability.** DataFly leverages GPU-accelerated rendering and scalable layout algorithms such as `sfdp` and `PivotMDS`. Scalability results are provided in [Sec. A7](#).

## 6 USABILITY STUDY AND RESULTS

To evaluate the practical utility of DataFly in helping users explore high-dimensional graph layouts (RQ2), we conducted a qualitative usability study with four participants via remote video conferencing using a screen-sharing and think-aloud protocol. Each 40–50 minute session comprised four phases: a pre-interview on the participant’s expertise, a tutorial video, hands-on exploration of a few datasets, and a closing Likert-scale questionnaire. During exploration, participants used the live system to perform open-ended exploration and tasks such as identifying nodes of interest, tracing neighbors, switching between projections, and comparing viewpoints across metrics, while verbalizing their observations.

**Participants.** We recruited four participants: two visualization experts (E1, E2), both PhD students who regularly work with graph data using tools such as NetworkX, Gephi, and D3. The other two participants were non-experts (N1, N2) with computer science backgrounds but no prior experience with graph embeddings or dimensionality reduction. This setup enabled us to evaluate DataFly’s accessibility to a broader audience. Datasets were selected by the participants to match their backgrounds: experts explored subsets of a VIS co-authorship network, a hypercube graph, a Game of Thrones character network, and a Last.fm music similarity network, while non-experts explored the Last.fm and Game of Thrones networks due to greater domain familiarity. None of the participants had prior exposure to DataFly.

**Expert feedback.** Both experts found the tool visually appealing and intuitive. E1 searched for recognizable node names and topological features, appreciating the ability to highlight and track nodes across projections, noting that “*in one layout a node looked like a neighbor, but in the other layout didn’t.*” They particularly valued the interactive rotation for resolving occlusion, finding that it revealed bridge connections between clusters that were hidden in static views. E1 also observed a duality between exploratory and communicative uses, noting that PCA viewpoints supported open-ended exploration while optimal projections could serve presentation: “*I like the duality of being able to explore, but also look at a layout that maybe is nice to present in a communication setting.*” On the hypercube dataset, they noted that higher-dimensional embeddings produced markedly different projections, whereas the traditional 2D layout made all views appear noisy and similar — “*in 2D, they all kind of look the same. It looks noisy.*”

E2 began by comparing layout algorithms and exploring the animated transitions. They found the transitions helpful for building intuition about the high-dimensional structure, though initially confused by the apparent rotation direction of the animations. They praised the metric chart for validating projection quality, finding it helpful to “*compare the values for the others as well.*” They also found the edge coloring scheme useful as a spatial anchor — when colors became “*all kind of messed up*” in a new projection, it prompted them to rotate the view to “*separate them back out again.*” On the music dataset, they remarked that thumbnails were effective for previewing and skipping uninformative projections.

Each expert proposed improvements: E1 suggested ego-network highlighting and edge tracking through transitions, while E2 recommended supporting additional graph formats.

**Non-expert feedback.** N1 started with the Last.fm network, independently noting its small-world structure. They went on to identify coherent genre clusters, pointing out a tight grouping of nu-metal and alternative metal bands, and used the rotation feature to position the cluster as visually salient.

N2 began with the Game of Thrones network, and made immediate comparisons with other 3D viewpoint editors, noting that the navigation controls of DataFly felt both natural and intuitive. Using the projection thumbnails to see different viewpoints, they noted that the separation between the Westeros and Essos storylines was visually salient across nearly all projections. They went on to explore the optimal projection and found the stress-optimized projection particularly informative. They also used the bookmark feature to save interesting viewpoints. Later in the session, they discovered the shift-click highlight feature on their own and found it valuable.

Both non-expert participants found similar insights in the Game of Thrones graph: both expressed surprise at the large number of connections of Robert Baratheon, and the unexpectedly small number of connections for many of the Stark family characters. Each participant used rotation and alternate projections to “convince” themselves of these observations, with N2 noting that they would not have believed this without the visualization. Both rated the tool’s visual appeal highly, with N1 noting that it felt “natural” and N2 praising its intuitive panning and rotation.

**Likert ratings.** Table 5 summarizes post-session ratings (1–5) across five aspects: *Intuitive* (how intuitive the tool is to use?), *Would Use* (how likely would you use the tool for work or personal interest),

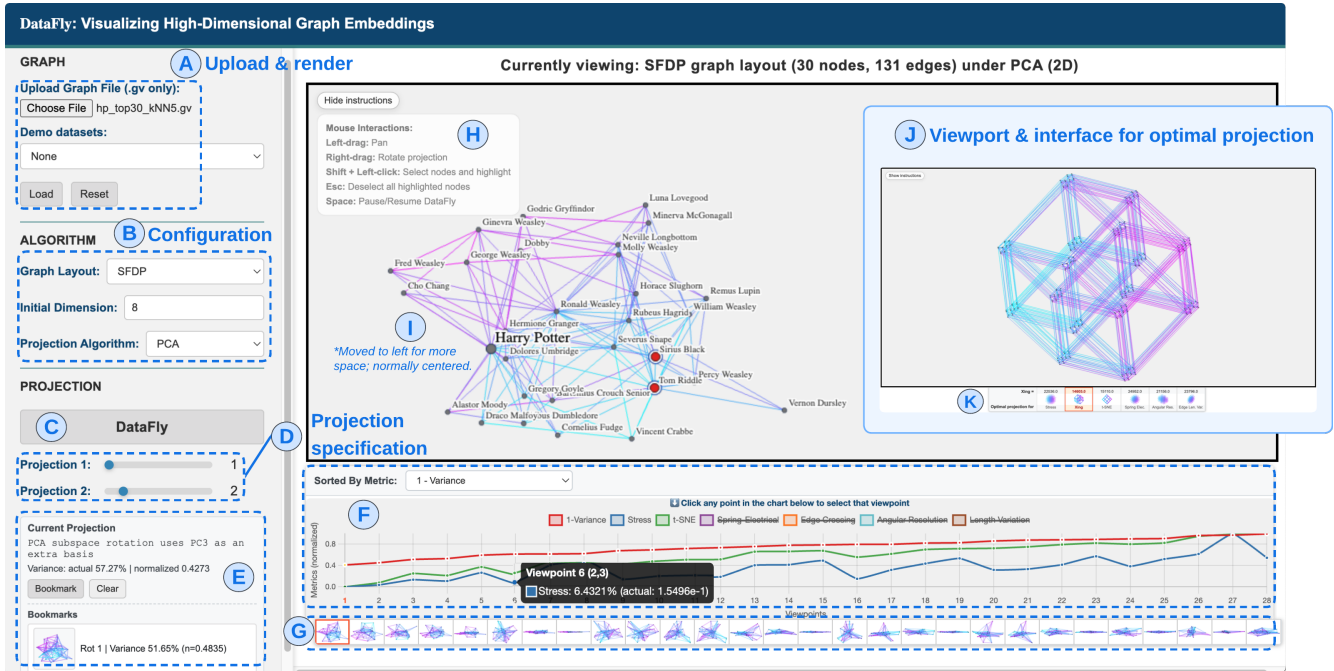


Fig. 6: DataFly interface and functionality overview. Main: Rotated PCA view of Harry Potter co-occurrence graph. Inset: Optimal Projection view of hypercube 8D.

Table 5: Likert-scale ratings (1 = poor, 5 = excellent) from all four participants.

Participant	Intuitive	Would Use	Appeal	Suitable	Interaction
Expert 1 (E1)	4	4	4	4	5
Expert 2 (E2)	4	3	5	4	4
Non-expert 1 (N1)	4	4	4	5	4
Non-expert 2 (N2)	2	2	5	4	5
Median	4	3.5	4.5	4	4.5

*Appeal* (overall visual appeal of the tool), *Suitable* (how suitable the tool is for answering questions about the data), and *Interaction* (overall effectiveness of the tool’s user interactions and instructions).

The tool received consistently high marks for visual appeal (median 4.5) and user interaction quality (median 4.5). Intuitiveness ratings were high among experts and N1 (all rated 4) but lower for N2 (rated 2), who struggled with interpreting the axes and viewpoints. Suitability scores were consistently high (median 4). Likelihood of use for work or personal interest varied (range 2–4).

**Results and findings summary.** The usability study indicates that DataFly helps users relate high-dimensional embeddings to recognizable structural patterns. Interactive rotation was repeatedly cited as essential for resolving occlusion and revealing otherwise hidden connections. Participants also valued the duality between exploratory and communicative uses: while PCA viewpoints supported open-ended exploration, the optimal projection mode was favored for producing aesthetic, presentation-ready layouts. Quantitatively, participants gave consistently high ratings for visual appeal, interaction quality, and task suitability. Based on participant feedback, we have iteratively improved the tool and outlined further updates in the Appendix (Sec. A8).

**Discussion on RQ2.** Taken together, the qualitative examples presented earlier (e.g., Figure 5), which demonstrate DataFly’s ability to reveal graph structures not visible in direct 2D layouts, along with the findings of this usability study, provide qualitative evidence supporting an affirmative answer to RQ2.

## 7 DISCUSSIONS AND LIMITATIONS

While DataFly currently supports viewpoints via linear projection, either optimized for one of the six metrics or allowing users to explore through the sequence of PCA projections, one might also consider non-linear projection techniques such as Multidimensional Scaling [44], t-SNE [47], or UMAP [49]. These methods can also produce a 2D representation of a high-dimensional graph layout, but they are less

suitable for the interactive exploration scenario considered here. First, they produce only a single projection for a fixed parameter setting, so exploring alternative views requires rerunning the method, potentially yielding layouts that differ significantly. Second, due to non-linearity, there is no meaningful relationship between two different embeddings. In this sense, non-linear projections are an abstract representation of high-dimensional data. DataFly allows users to explore, in a principled way, several viewpoints of a high-dimensional graph embedding using interpretable linear projection techniques.

Due to Graphviz limitations, our experiments were restricted to layouts up to 10 dimensions; future work will investigate whether higher-dimensional layouts provide additional benefits.

## 8 CONCLUSIONS

This paper proposes an approach to graph visualization that embeds graphs in high-dimensional space and systematically searches for informative 2D viewpoints, moving beyond the conventional paradigm of producing a single static 2D layout.

Our experimental results show that optimal projections derived from high-dimensional embeddings can produce superior visualizations, with metrics (e.g., edge crossings) outperforming 2D layout algorithms such as SGD<sup>2</sup> and SmartGD which are explicitly designed to minimize them. DataFly also reveals structural patterns not apparent in widely used 2D layouts such as `neato` and `sfdp`. We further introduce SigmoidX, an effective differentiable loss function for edge crossings that is simpler to implement than the neural network–based surrogate used in SGD<sup>2</sup>, while achieving significantly fewer crossings than both SGD<sup>2</sup> and SmartGD in our experiments.

To make these high-dimensional embeddings accessible to users, we propose an interactive tool DataFly for exploring high-dimensional graph embeddings and discovering insights. The system enables users to find projections that optimize specific metrics or explore a set of PCA-based viewpoints, accompanied by a chart displaying quality metrics such as stress, t-SNE score, and edge crossings. Users can interactively explore the high-dimensional layout landscape by “flying” from one viewpoint to another. Our usability study with experts and non-experts provides encouraging evidence that DataFly helps users discover structural patterns that remain hidden in conventional 2D layouts.

## ACKNOWLEDGMENTS

The authors thank Pan Xu for her input during the initial exploration of this project.

## REFERENCES

- [1] R. Ahmed, F. De Luca, S. Devkota, S. Kobourov, and M. Li. Multicriteria scalable graph drawing via stochastic gradient descent,  $(SGD)^2$ . *IEEE Transactions on Visualization and Computer Graphics*, 28(6):2388–2399, 2022. doi: 10.1109/TVCG.2022.3155564 2, 4, 6
- [2] E. Argyriou, M. Bekos, and A. Symvonis. Maximizing the total resolution of graphs. In U. Brandes and S. Cornelsen, eds., *Graph Drawing*, vol. 6502 of *Lecture Notes in Computer Science*, pp. 62–67. Springer, 2011. doi: 10.1007/978-3-642-18469-7\_6 2
- [3] G. D. Battista, A. Garg, G. Liotta, R. Tamassia, E. Tassinari, and F. Vargiu. An experimental comparison of four graph drawing algorithms. *CGTA: Computational Geometry: Theory and Applications*, 7:303–325, 1997. doi: 10.1016/S0925-7721(96)00005-3 4
- [4] M. Behrisch, B. Bach, M. Hund, M. Delz, L. von R'uden, J.-D. Fekete et al. Magnostics: Image-based search of interesting matrix views for guided network exploration. *IEEE Transactions on Visualization and Computer Graphics*, 23(1):31–40, 2017. doi: 10.1109/TVCG.2016.2598467 18
- [5] M. A. Bekos, H. Förster, C. Geckeler, L. Holländer, M. Kaufmann, A. M. Spallek et al. A heuristic approach towards drawings of graphs with high crossing resolution. *The Computer Journal*, 64(1):7–26, 2021. doi: 10.1093/COMJNL/BXZ133 2
- [6] E. Bertini and G. Santucci. Visual quality metrics. In *Proceedings of the 2006 AVI Workshop on BEyond Time and Errors: Novel Evaluation Methods for Information Visualization (BELIV)*, pp. 1–5. ACM, Venice, Italy, 2006. doi: 10.1145/1168149.1168159 18
- [7] A. Bezerianos, F. Chevalier, P. Dragicicvic, N. Elmqvist, and J.-D. Fekete. Graphdice: A system for exploring multivariate social networks. *Computer Graphics Forum*, 29(3):863–872, 2010. doi: 10.1111/j.1467-8659.2009.01687.x 2
- [8] U. Brandes and C. Pich. Eigensolver methods for progressive multidimensional scaling of large data. In *Proc. 14th Intl. Symp. Graph Drawing (GD '06)*, vol. 4372 of *LNCS*, pp. 42–53, 2007. doi: 10.1007/978-3-540-70904-6\_6 3
- [9] A. Buja, D. Cook, and D. F. Swayne. Interactive high-dimensional data visualization. *Journal of Computational and Graphical Statistics*, 5(1):78–99, 1996. doi: 10.1080/10618600.1996.10474696 2
- [10] W. Castelein, Z. Tian, T. Mchedlidze, and A. C. Telea. Viewpoint-based quality for analyzing and exploring 3d multidimensional projections. In *VISIGRAPP (3: IVAPP)*, pp. 65–76, 2023. doi: 10.5220/0011652800003417 2
- [11] M. Chimani, P. Eades, P. Eades, S.-H. Hong, W. Huang, K. Klein et al. People prefer less stress and fewer crossings. In C. Duncan and A. Symvonis, eds., *Graph Drawing*, vol. 8871 of *LNCS*, pp. 523–524. Springer, 2014. 3
- [12] M. Chimani, C. Gutwenger, M. Jünger, G. W. Klau, K. Klein, and P. Mutzel. The open graph drawing framework (ogdf). In R. Tamassia, ed., *Handbook of Graph Drawing and Visualization*, chap. 17, pp. 443–505. CRC Press, 2014. 3
- [13] D. Cook, A. Buja, J. Cabrera, and C. Hurley. Grand tour and projection pursuit. *Journal of Computational and Graphical Statistics*, 4(3):155–172, 1995. doi: 10.2307/1390769 2, 18
- [14] R. Cutura, S. Holzer, M. Aupetit, and M. Sedlmair. Viscoder: A tool for visually comparing dimensionality reduction algorithms. In *Euro. Symp. Artificial Neural Networks, Computational Intelligence and Machine Learning*, pp. 641–646, 4 2018. 2
- [15] T. N. Dang and L. Wilkinson. Scagexplorer: Exploring scatterplots by their scagnostics. In *Proceedings of the IEEE Pacific Visualization Symposium (PacificVis)*, pp. 73–80. IEEE, 2014. doi: 10.1109/PacificVis.2014.6787139 2
- [16] T. Davis and Y. Hu. University of Florida Sparse Matrix Collection. *ACM Transactions on Mathematical Software*, 38:1–25, 2011. <http://www.cise.ufl.edu/research/sparse/matrices/>. doi: 10.1145/2049662.2049663 4
- [17] S. Devkota, R. Ahmed, F. De Luca, K. E. Isaacs, and S. Kobourov. Stress-plus-x (SPX) graph layout. In *Prof. Springer International Symposium on Graph Drawing and Network Visualization*, pp. 291–304, 2019. doi: 10.1007/978-3-030-35802-0\_23 2
- [18] W. Didimo, G. Liotta, and S. Romeo. Topology-driven force-directed algorithms. *Proc. of GD 2010*, 6502:165–176, 09 2010. doi: 10.1007/978-3-642-18469-7\_15 2
- [19] T. Dwyer, B. Lee, D. Fisher, K. I. Quinn, P. Isenberg, G. Robertson et al. A comparison of user-generated and automatic graph layouts. *IEEE Transactions on Visualization and Computer Graphics*, 15(6):961–968, 2009. doi: 10.1109/TVCG.2009.109 6
- [20] P. Eades. A heuristic for graph drawing. *Congressus Numerantium*, 42:149–160, 1984. 2, 4
- [21] M. Espadoto, R. M. Martins, A. Kerren, N. S. T. Hirata, and A. C. Telea. Toward a quantitative survey of dimension reduction techniques. *IEEE Trans. Vis. Comput. Graph.*, 27(3):2153–2173, 2021. doi: 10.1109/TVCG.2019.2944182 2
- [22] R. Etemadpour, R. C. da Motta, J. G. de Souza Paiva, R. Minghim, M. C. F. de Oliveira, and L. Linsen. Perception-based evaluation of projection methods for multidimensional data visualization. *IEEE Transactions on Visualization and Computer Graphics*, 21(1):81–94, 2015. doi: 10.1109/TVCG.2014.2346451 2
- [23] T. M. J. Fruchterman and E. M. Reingold. Graph drawing by force directed placement. *Software - Practice and Experience*, 21:1129–1164, 1991. doi: 10.1002/spe.4380211102 2, 4
- [24] M. Gaertler and M. Krug. Flying through a graph's spectrum. In *13th International Symposium (GD)*, pp. 528–531, 2005. 2
- [25] P. Gajer, M. T. Goodrich, and S. G. Kobourov. A multi-dimensional approach to force-directed layouts of large graphs. In J. Marks, ed., *Graph Drawing - 8th International Symposium, GD 2000, Proceedings*, vol. 1984 of *LNCS*, pp. 211–221. Springer-Verlag, 2001. doi: 10.1007/3-540-44541-2\_20 1, 2, 4
- [26] E. R. Gansner, Y. Koren, and S. North. Graph drawing by stress majorization. In *Proc. Springer International Symposium on Graph Drawing*, pp. 239–250, 2004. doi: 10.1007/978-3-540-31843-9\_25 2, 4
- [27] E. R. Gansner, Y. Koren, and S. C. North. Graph drawing by stress majorization. In *Proc. 12th Intl. Symp. Graph Drawing (GD '04)*, vol. 3383 of *LNCS*, pp. 239–250. Springer, 2004. doi: 10.1007/978-3-540-31843-9\_25 3
- [28] I. Goodfellow, Y. Bengio, and A. Courville. *Deep Learning*. MIT Press, 2016. 5
- [29] R. Gove. Gragnostics: Fast, interpretable features for comparing graphs. In *23rd International Conference on Information Visualisation (IV)*, pp. 201–209. IEEE, 2019. doi: 10.1109/IV.2019.00042 18
- [30] Graphviz. <http://graphviz.org>. 3
- [31] A. Hagberg, P. Swart, and D. Chult. Exploring network structure, dynamics, and function using networkx. 01 2008. doi: doi.org/10.25080/tcww9851 3
- [32] K. M. Hall. An  $r$ -dimensional quadratic placement algorithm. *Management Science*, 17:219–229, 1970. doi: 10.1287/mnsc.17.3.219 3
- [33] N. Henry, J.-D. Fekete, and M. J. McGuffin. NodeTriX: A hybrid visualization of social networks. *IEEE Transactions on Visualization and Computer Graphics*, 13(6):1302–1309, 2007. doi: 10.1109/TVCG.2007.70582 18
- [34] H. Hotelling. Analysis of a complex of statistical variables into principal components. *Journal of Educational Psychology*, 24:417–441, 498–520, 1933. doi: 10.1037/h0071325 5, 7
- [35] Y. Hu. Efficient and high quality force-directed graph drawing. *Mathematica Journal*, 10:37–71, 2005. 3
- [36] Y. Hu. Algorithms for visualizing large networks. In U. Naumann and O. Schenk, eds., *Combinatorial Scientific Computing*, pp. 525–549. CRC Press, 2012. 3
- [37] M. Y. Huh and K. Kim. Visualization of multidimensional data using modifications of the grand tour. *Journal of Applied Statistics*, 29(5):721–728, 2002. doi: 10.1080/02664760120098784 2
- [38] A. Jolicœur-Martineau. The relativistic discriminator: a key element missing from standard gan. *arXiv preprint arXiv:1807.00734*, 2018. 6
- [39] L. Joos, G. J. Mooney, M. T. Fischer, D. A. Keim, F. Schreiber, H. C. Purchase et al. Show me your best side: Characteristics of user-preferred perspectives for 3d graph drawings. In *33rd International Symposium on Graph Drawing and Network Visualization (GD 2025)*, vol. 357 of *Leibniz International Proceedings in Informatics (LIPIcs)*, pp. 37:1–37:19. Schloss Dagstuhl – Leibniz-Zentrum für Informatik, 2025. doi: 10.4230/LIPIcs.GD.2025.37 2
- [40] T. Kamada and S. Kawai. An algorithm for drawing general undirected graphs. *Information Processing Letters*, 31(1):7–15, 1989. doi: 10.1016/0020-0190(89)90102-6 2

- [41] D. P. Kingma and J. Ba. Adam: A method for stochastic optimization. *arXiv preprint arXiv:1412.6980*, 2014. 4
- [42] S. G. Kobourov. Force-directed drawing algorithms. *Handbook of Graph Drawing and Visualization*, pp. 383–408, 2013. doi: 10.1201/b15385-15 2, 3
- [43] Y. Koren. On spectral graph drawing. In *COCOON*, 2003. doi: 10.1007/3-540-45071-8\_50 1
- [44] J. B. Kruskal. Multidimensional scaling by optimizing goodness of fit to a nonmetric hypothesis. *Psychometrika*, 29:1–27, 1964. doi: 10.1007/BF02289565 9
- [45] U. Laa. High-dimensional data visualisation with the grand tour. In *EPJ Web of Conferences*, vol. 245, p. 06018. EDP Sciences, 2020. 24th International Conference on Computing in High Energy and Nuclear Physics (CHEP 2019), Section 6 - Physics Analysis, 6 pages, published online 16 November 2020. doi: 10.1051/epjconf/202024506018 2
- [46] M. Li, Z. Zhao, and C. Scheidegger. Visualizing neural networks with the grand tour. *Distill*, 2020. <https://distill.pub/2020/grand-tour>. doi: 10.23915/distill.00025 2
- [47] L. v. Maaten and G. Hinton. Visualizing data using t-SNE. *Journal of Machine Learning Research*, 9:2579–2605, 2008. 3, 9
- [48] R. M. Martins, H. Heberle, G. Andery, F. Paulovich, et al. Multidimensional projections for visual analysis of social networks. *Journal of Computer Science and Technology*, 27(4):791–810, July 2012. doi: 10.1007/s11390-012-1265-5 2
- [49] L. McInnes, J. Healy, and J. Melville. Umap: Uniform manifold approximation and projection for dimension reduction, 2018. cite arxiv:1802.03426Comment: Reference implementation available at <http://github.com/lmcinnes/umap>. 9
- [50] G. J. Mooney, J. Miller, M. Wybrow, S. Kobourov, and H. C. Purchase. Stress in graph drawings: Perception, preference, and performance. In *33rd International Symposium on Graph Drawing and Network Visualization (GD 2025)*, vol. 357 of *Leibniz International Proceedings in Informatics (LIPIcs)*, pp. 38:1–38:23. Schloss Dagstuhl – Leibniz-Zentrum für Informatik, 2025. doi: 10.4230/LIPIcs.GD.2025.38 3
- [51] C. Morariu, A. Bibal, R. Cutura, B. Frénay, and M. Sedlmair. Predicting user preferences of dimensionality reduction embedding quality. *IEEE Transactions on Visualization and Computer Graphics*, 29(1):745–755, 2023. doi: 10.1109/TVCG.2022.3209449 2
- [52] L. G. Nonato and M. Aupetit. Multidimensional projection for visual analytics: Linking techniques with distortions, tasks, and layout enrichment. *IEEE Trans. Vis. Comput. Graph.*, 25(8):2650–2673, 2019. doi: 10.1109/TVCG.2018.2846735 2
- [53] F. V. Paulovich, A. Arleo, and S. van den Elzen. When dimensionality reduction meets graph (drawing) theory: Introducing a common framework, challenges and opportunities. *Computer Graphics Forum*, 44(3):e70105, 2025. doi: 10.1111/cgf.70105 2
- [54] H. C. Purchase. Which aesthetic has the greatest effect on human understanding? In G. DiBattista, ed., *Proc. 5th Intl. Symp. Graph Drawing (GD '97)*, vol. 1353 of *LNCS*, pp. 248–261. Springer-Verlag, 1997. doi: 10.1007/3-540-63938-1\_67 6
- [55] M. Radermacher, K. Reichard, I. Rutter, and D. Wagner. Geometric heuristics for rectilinear crossing minimization. *ACM J. Exp. Algorithmics*, 24, art. no. 1.12, 21 pages, 2019. doi: 10.1145/3325861 2
- [56] M. Radermacher, K. Reichard, I. Rutter, and D. Wagner. Geometric heuristics for rectilinear crossing minimization. *Journal of Experimental Algorithmics (JEA)*, 24:1–21, 2019. doi: 10.1145/3325861 2, 6, 7
- [57] K. Smelser, K. Gunaratne, J. Miller, and S. Kobourov. How scale breaks “normalized stress” and KL divergence: Rethinking quality metrics. *IEEE Transactions on Visualization and Computer Graphics*, 2026. doi: 10.1109/TVCG.2026.3657654 3
- [58] D. Smilkov, N. Thorat, C. Nicholson, E. Reif, F. B. Viégas, and M. Wattenberg. Embedding projector: Interactive visualization and interpretation of embeddings. *arXiv preprint arXiv:1611.05469*, 2016. 2
- [59] W. C. Ticona, N. Boukhelifa, and E. Lutton. Evographdice: Interactive evolution for visual analytics. In *Proceedings of the IEEE Congress on Evolutionary Computation*, pp. 1–8, 2012. doi: 10.1109/CEC.2012.6256553 2
- [60] W. S. Torgerson. Multidimensional scaling: I. theory and method. *Psychometrika*, 17:401–419, 1952. doi: 10.1007/BF02288916 3
- [61] W. Tutte. How to draw a graph. *Proceedings of the London Mathematical Society*, 13:743–768, 1963. 2
- [62] S. van Wageningen, T. Mchedlidze, and A. C. Telea. Viewpoint optimization for 3d graph drawings. *Computer Graphics Forum*, 44(3), 2025. doi: 10.1111/CGF.70127 1, 2
- [63] X. Wang, K. Yen, Y. Hu, and H.-W. Shen. DeepGD: A deep learning framework for graph drawing using GNN. *IEEE Computer Graphics and Applications*, 41(5):32–44, 2021. doi: 10.1109/MCG.2021.3093908 4
- [64] X. Wang, K. Yen, Y. Hu, and H.-W. Shen. SmartGD: A GAN-based graph drawing framework for diverse aesthetic goals. *IEEE Transactions on Visualization and Computer Graphics*, 30(8):5666–5678, 2024. doi: 10.1109/TVCG.2023.3306356 2, 3, 4, 6
- [65] M. Wattenberg. Visual exploration of multivariate graphs. In *Proceedings of the international conference on human factors in computing systems (CHI'06)*, pp. 811–819, 2006. doi: 10.1145/1124772.1124891 1
- [66] R. Wiese, M. Eiglsperger, and M. Kaufmann. *yFiles — Visualization and Automatic Layout of Graphs*, pp. 173–191. Springer Berlin Heidelberg, 2004. 3
- [67] J. X. Zheng, S. Pawar, and D. M. Goodman. Graph drawing by stochastic gradient descent. *IEEE Transactions on Visualization and Computer Graphics*, 25(09):2738–2748, sep 2019. doi: 10.1109/TVCG.2018.2859997 2

## APPENDIX

### A1 DIFFERENTIABLE SURROGATE FUNCTION FOR EDGE CROSSING

We define a differentiable approximation for detecting whether two edges intersect as follows.

Let the two edges be

$$e_1 : p + tr, \quad e_2 : q + us, \quad t, u \in [0, 1],$$

where  $p, q \in \mathbb{R}^2$  are the start points, and  $r, s$  are the direction vectors. The endpoints of these two edges are  $p + r$  and  $q + s$ .

The intersection parameters are computed as

$$t = \frac{(q-p) \times s}{r \times s}, \quad u = \frac{(q-p) \times r}{r \times s},$$

where “ $\times$ ” denotes the 2D cross product. Geometrically, when  $t \in [0, 1]$ , it means that  $e_2$ , or its extension, hits  $e_1$ . Similarly,  $u \in [0, 1]$  means that  $e_1$ , or its extension, hits  $e_2$ . Hence, if the two edges cross, we must have  $t, u \in [0, 1]$ .

Instead of using a hard condition ( $t, u \in [0, 1]$ ) to decide whether the edges intersect, which is not differentiable, we use sigmoid-based soft masks:

$$M_t = \frac{\sigma_T(t)[1 - \sigma_T(t-1)]}{M_{\text{peak}}}, \quad M_u = \frac{\sigma_T(u)[1 - \sigma_T(u-1)]}{M_{\text{peak}}},$$

where  $\sigma_T(u) = 1/(1 + e^{-Tu})$  is the sigmoid function with temperature  $T$  (we use  $T = 10$ ), and  $M_{\text{peak}} = \sigma_T(0.5)[1 - \sigma_T(-0.5)]$  normalizes the peak value.

The differentiable edge-crossing probability is

$$P(\text{crossing}) = M_t M_u,$$

which approaches 1 when the edges intersect ( $t, u \in [0, 1]$ ) and smoothly decreases toward 0 otherwise. We call this loss function *SigmoidX*. It is a continuous, differentiable proxy for the binary “edges intersect” test, enabling gradient-based optimization to minimize edge crossings. We also experimented with other surrogate functions, including a pyramid function over the unit square, but found that *SigmoidX* performs better.

### A2 SCALE-INVARIANT SPRING-ELECTRICAL ENERGY

This metric treats edges as springs and nodes as electrically repelling particles and measures the energy of the system:

$$\text{se\_eng}(x) = \sum_{(i,j) \in E} \frac{\|\mathbf{x}_i - \mathbf{x}_j\|^3}{3K_s} - \sum_{i \neq j} K_r \ln(\|\mathbf{x}_i - \mathbf{x}_j\|).$$

where  $K_s$  and  $K_r$  are spring and repulsion constants. We set them to 1. To make this metric scale-invariant, we can find a scaling factor  $t$  such that  $\text{se\_eng}(tx)$  is minimized. If we denote the first term in the energy as  $A/3$  (for attractive spring energy) and the second as  $R$  (repulsive electrical energy), then we want to minimize

$$\text{se\_eng}(tx) = \frac{A}{3}t^3 - R - \ln(t) * M$$

where  $M = |V|(|V| - 1)$ . Taking the derivative and setting it to zero, the optimum is achieved when  $t = (\frac{M}{A})^{1/3}$ . The final energy is

$$\begin{aligned} \text{se\_eng}(x) &= \frac{M}{3} + \frac{M}{3} \ln \frac{A}{M} - R \\ &= \frac{|V|(|V| - 1)}{3} + \frac{|V|(|V| - 1)}{3} \ln \frac{\sum_{(i,j) \in E} \|\mathbf{x}_i - \mathbf{x}_j\|^3}{|V|(|V| - 1)} \\ &\quad - \sum_{i \neq j} \ln(\|\mathbf{x}_i - \mathbf{x}_j\|) \end{aligned}$$

### A3 ADDITIONAL RESULTS FOR NEATO

Tables A1-A2 show visualizations of graphs in the Rome20 dataset, comparing *neato* with DataFly’s optimal projection  $\text{DF}_{\text{opt}}^{\text{neato}}$  across various metrics. The corresponding metric values for *neato* and  $\text{DF}_{\text{opt}}^{\text{neato}}$  are shown below each visualization. Because  $\text{DF}_{\text{opt}}^{\text{neato}}$  is a projection of a high-dimensional *neato* layout, its drawings remain visually similar to those of *neato*, yet apart from stress and spring-electrical loss,  $\text{DF}_{\text{opt}}^{\text{neato}}$  typically achieves better metric values. For example, for grafo11543,  $\text{DF}_{\text{opt}}^{\text{neato}}$  find a planar layout, whereas *neato* has four edge crossings.

Table A3 presents the stress achieved by *neato* when optimizing directly in various dimensions from 2D to 10D. As expected, stress is significantly lower in 10D for all graphs.

### A4 ADDITIONAL RESULTS FOR SFDP

Table A4 presents visualizations produced by *sfdp* on the SuiteSparse14 dataset. Optimizing different metrics results in markedly different layouts. For example, optimizing edge crossings (*xing*) produces a layout that differs substantially from the default *sfdp* output. Optimizing the t-SNE metric yields a visually less complex layout that appears to contain fewer edge crossings; however, closer inspection reveals many crossings hidden at finer scales.

Table A5 presents the stress achieved by *sfdp* when optimizing directly in various dimensions from 2D to 10D. It is surprising that the spring-electrical energy obtained by *sfdp* (10) is mostly similar to that for *sfdp* (2), except for the Journals graph. Furthermore, the spring-electrical loss by  $\text{DF}_{\text{opt}}^{\text{sfdp}}$  and  $\text{DF}_{\text{PCA}}^{\text{sfdp}}$  are also quite similar to that of *neato*. This seems to indicate that optimal layout for this loss function can be realized well in lower dimension.

One way to decide whether a high-dimensional embedding can “live” happily in a lower-dimensional hyperplane is to look at the variance explained by PCA projections at a lower dimension. This is confirmed in Table A6, where we looked at variance explained for SuiteSparse14 graphs by PCA projection from 10D of *sfdp* vs *neato*. We can see that the variance explained for *sfdp* is indeed higher than for *neato*, at the same layout dimension. E.g., PCA projection of 10D embeddings to 3D can explain 87.8% of the original variance, vs 82.5% for *neato*.

### A5 STATISTICAL SIGNIFICANCE OF OUTPERFORMANCE OF $\text{DF}_{\text{opt}}^{\text{NEATO}}$ AND $\text{DF}_{\text{PCA}}^{\text{SFDP}}$

Figure A1 (top) shows paired-bootstrap ( $n = 5000$ ) 95% confidence intervals (CIs) for the SPC metric across various evaluation measures. When a CI lies entirely below 0, it indicates that  $\text{DF}_{\text{opt}}^{\text{neato}}$  outperforms *neato* with statistical significance (confirmed via a two-sided bootstrap test). Under this view,  $\text{DF}_{\text{opt}}^{\text{neato}}$  clearly outperforms in angular resolution, t-SNE score, and edge crossings. Paired-bootstrap 95% confidence intervals (CIs) for the SPC metric across various evaluation measures are given in Figure A2 in the Appendix. We see that the outperformance of  $\text{DF}_{\text{opt}}^{\text{sfdp}}$  over *sfdp* in angular resolution and edge length variation is statistically significant.

Additional CIs for the other comparisons are shown in Figures A3 and A4. Most of the differences are clear, except for  $\text{DF}_{\text{opt}}^{\text{neato}}$  and SmartGD in crossings compared to  $\text{SGD}^2$ . Here, the SmartGD interval intersects 0, suggesting that there may be no difference in overall performance in crossing minimization between these graphs. The  $\text{DF}_{\text{opt}}^{\text{neato}}$  interval is close, but does not contain 0. If we compute a  $p$ -value for whether the mean SPC between the algorithms is 0, we get 0.0394.

### A6 SYSTEM DETAILS

The system uses a Python/Flask backend with SocketIO for real-time communication, and a JavaScript/HTML/CSS frontend featuring 3D graph visualization via Three.js and interactive metric charts with Chart.js.

We improve efficiency and flexibility through on-demand metric computation and lazy loading. Expensive metrics like t-SNE are computed and loaded only when requested via asynchronous API calls,

Table A1: Optimal projections of the 10D Neato layout of the Rome20 dataset (part 1/2). Numbers show Neato vs.  $DF_{opt}^{neato}$  metrics. **Bold** = better. Edges colored by length: **red** = short, **blue** = long.

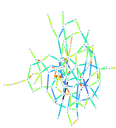
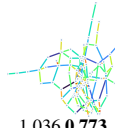
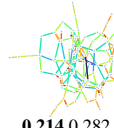
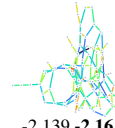
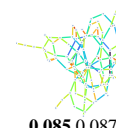
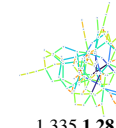
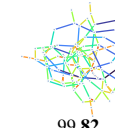
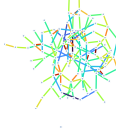
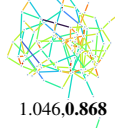
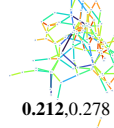
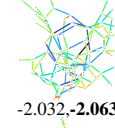
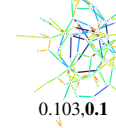
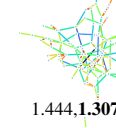
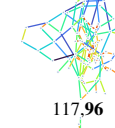

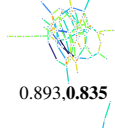
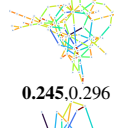
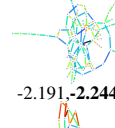
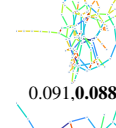
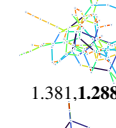
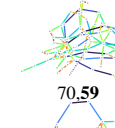



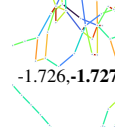


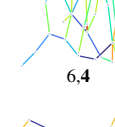





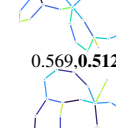
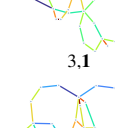
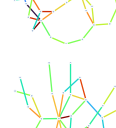


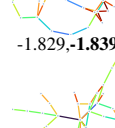
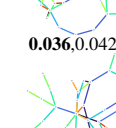
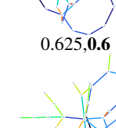
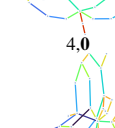
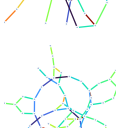

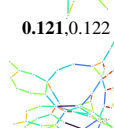

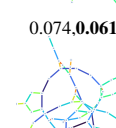
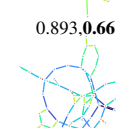

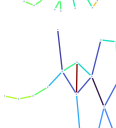



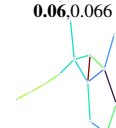
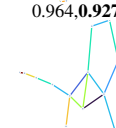

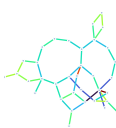

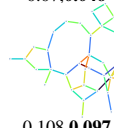
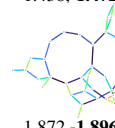
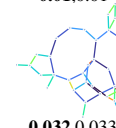
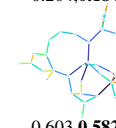








	neato	ang_res↓	edge_len↓	spr_elec↓	stress↓	tsne↓	xing↓
grafo10379.95							
		1.036, <b>0.773</b>	<b>0.214</b> ,0.282	-2.139,- <b>2.16</b>	<b>0.085</b> ,0.087	1.335, <b>1.28</b>	<b>99.82</b>
grafo10451.95							
		1.046, <b>0.868</b>	<b>0.212</b> ,0.278	-2.032,- <b>2.063</b>	0.103, <b>0.1</b>	1.444, <b>1.307</b>	<b>117.96</b>
grafo10480.95							
		0.893, <b>0.835</b>	<b>0.245</b> ,0.296	-2.191,- <b>2.244</b>	0.091, <b>0.088</b>	1.381, <b>1.288</b>	<b>70.59</b>
grafo11311.40							
		0.87, <b>0.696</b>	<b>0.196</b> ,0.216	-1.726,- <b>1.727</b>	<b>0.066</b> ,0.073	0.784, <b>0.716</b>	<b>6.4</b>
grafo11412.32							
		0.842, <b>0.696</b>	<b>0.101</b> ,0.116	-1.979,- <b>2.035</b>	<b>0.032</b> ,0.033	0.569, <b>0.512</b>	<b>3.1</b>
grafo11543.34							
		0.872, <b>0.753</b>	<b>0.092</b> ,0.174	-1.829,- <b>1.839</b>	<b>0.036</b> ,0.042	0.625, <b>0.6</b>	<b>4.0</b>
grafo11674.33							
		0.924, <b>0.615</b>	<b>0.121</b> ,0.122	-1.611,- <b>1.713</b>	0.074, <b>0.061</b>	0.893, <b>0.66</b>	<b>11.3</b>
grafo1583.66							
		0.815, <b>0.704</b>	<b>0.186</b> ,0.245	- <b>2.253</b> ,-2.252	<b>0.06</b> ,0.066	0.964, <b>0.927</b>	<b>13.12</b>
grafo2747.16							
		0.845, <b>0.635</b>	0.07, <b>0.046</b>	-1.438,- <b>1.472</b>	<b>0.01</b> ,0.01	0.204, <b>0.184</b>	<b>0.0</b>
grafo2815.35							
		0.934, <b>0.7</b>	0.108, <b>0.097</b>	-1.872,- <b>1.896</b>	<b>0.032</b> ,0.033	0.603, <b>0.582</b>	<b>5.2</b>

Table A2: Optimal projections of the 10D Neato layout of the Rome20 dataset (part 2/2). Numbers show Neato vs.  $DF_{opt}^{neato}$  metrics. **Bold** = better. Edges colored by length: **red** = short, **blue** = long.

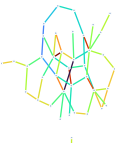
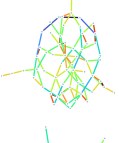
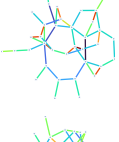
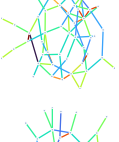
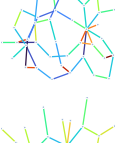
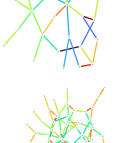
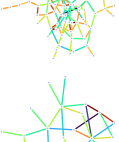
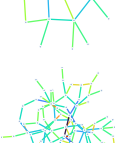
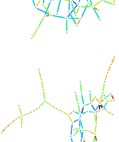

	neato	ang_res↓	edge_len↓	spr_elec↓	stress↓	tsne↓	xing↓
grafo2955.38		0.96, <b>0.754</b>	<b>0.153</b> ,0.217	-1.692,- <b>1.7</b>	<b>0.063</b> ,0.07	0.78, <b>0.708</b>	<b>9.6</b>
grafo3138.60		1.137, <b>0.889</b>	0.244, <b>0.226</b>	- <b>1.809</b> ,-1.791	<b>0.089</b> ,0.095	1.054, <b>1.0</b>	<b>42.31</b>
grafo3587.36		1.186, <b>0.868</b>	0.176, <b>0.173</b>	-1.748,- <b>1.755</b>	<b>0.041</b> ,0.046	<b>0.621</b> ,0.669	<b>6.7</b>
grafo5780.48		1.143, <b>0.886</b>	0.221, <b>0.203</b>	-1.657,- <b>1.672</b>	<b>0.086</b> ,0.089	0.972, <b>0.892</b>	<b>41.25</b>
grafo7023.45		0.913, <b>0.718</b>	<b>0.156</b> ,0.194	-1.836,- <b>1.84</b>	<b>0.063</b> ,0.069	0.886, <b>0.816</b>	<b>15.8</b>
grafo762.27		0.807, <b>0.568</b>	<b>0.123</b> ,0.157	-1.544,- <b>1.567</b>	<b>0.052</b> ,0.057	0.579, <b>0.554</b>	<b>3.3</b>
grafo8296.86		0.964, <b>0.771</b>	<b>0.214</b> ,0.24	-2.071,- <b>2.079</b>	<b>0.092</b> ,0.102	1.361, <b>1.257</b>	<b>81.66</b>
grafo847.22		1.136, <b>0.622</b>	0.121, <b>0.051</b>	- <b>1.257</b> ,-1.257	<b>0.051</b> ,0.056	0.421, <b>0.373</b>	<b>4.4</b>
grafo9033.80		1.025, <b>0.778</b>	<b>0.219</b> ,0.279	-2.066,- <b>2.079</b>	<b>0.083</b> ,0.09	1.235, <b>1.138</b>	<b>61.54</b>
grafo9592.72		0.859, <b>0.692</b>	<b>0.142</b> ,0.204	-2.584,- <b>2.66</b>	<b>0.037</b> ,0.044	0.913, <b>0.845</b>	<b>16.13</b>

Table A3: Stress for Neato layouts at different dimensions, vs that for the Optimal projection to 2D, and for the best PCA projection to 2D.

	neato at K					OptProj (from K-D to 2D)				PCA (from K-D to 2D)			
	2	3	5	7	10	3	5	7	10	3	5	7	10
1138_bus	0.069	0.030	0.013	0.008	<b>0.006</b>	0.074	0.083	0.080	0.076	0.075	0.087	0.101	0.113
bcsprw07	0.046	0.022	0.010	0.007	<b>0.006</b>	0.057	0.062	0.063	0.062	0.058	0.068	0.074	0.077
email	0.133	0.085	0.047	0.033	<b>0.025</b>	0.145	0.157	0.156	0.163	0.145	0.159	0.165	0.171
Erdos991	0.109	0.063	0.033	0.023	<b>0.017</b>	0.124	0.131	0.131	0.129	0.125	0.143	0.150	0.161
EX1	0.167	0.103	0.050	0.035	<b>0.033</b>	0.169	0.173	0.176	0.176	0.169	0.177	0.177	0.177
football	0.128	0.077	0.043	0.036	<b>0.032</b>	0.132	0.133	0.133	0.132	0.132	0.134	0.136	0.139
hypercube10	0.198	0.135	0.081	0.058	<b>0.041</b>	0.199	0.202	0.204	0.206	0.199	0.202	0.205	0.208
Journals	0.167	0.114	0.071	0.055	<b>0.043</b>	0.176	0.180	0.185	0.182	0.178	0.182	0.194	0.198
mobius	0.029	0.017	<b>0.016</b>	<b>0.016</b>	<b>0.016</b>	0.035	0.036	0.036	0.034	0.042	0.043	0.043	0.043
qh882	0.056	0.028	0.014	0.010	<b>0.009</b>	0.069	0.071	0.074	0.072	0.072	0.080	0.087	0.089
Si2	0.159	0.088	0.050	0.036	<b>0.027</b>	0.139	0.142	0.143	0.143	0.139	0.142	0.143	0.144
spiral	0.044	0.025	0.017	0.014	<b>0.012</b>	0.053	0.064	0.064	0.062	0.054	0.064	0.075	0.078
Trefethen_700	0.177	0.118	0.072	0.055	<b>0.044</b>	0.178	0.180	0.181	0.181	0.180	0.197	0.207	0.218
USpowerGrid	0.058	0.028	0.011	0.007	<b>0.005</b>	0.066	0.074	0.077	0.073	0.066	0.077	0.082	0.086
SPC	0	-0.459	-0.707	-0.794	<b>-0.844</b>	0.088	0.122	0.127	0.122	0.088	0.136	0.163	0.176

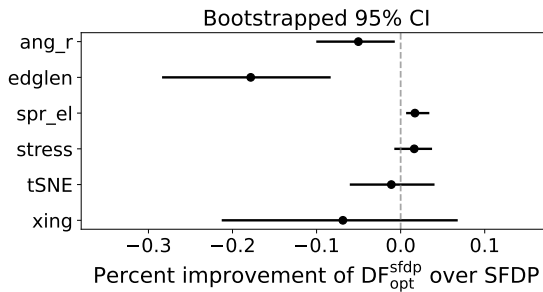
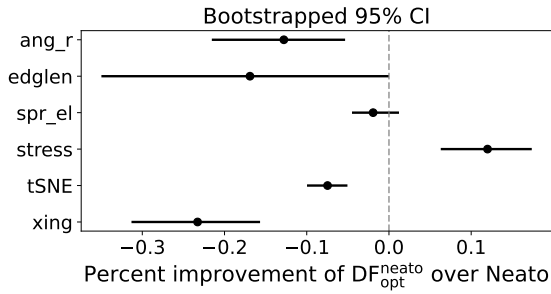


Fig. A1: Bootstrapped 95% confidence intervals for  $DF_{opt}^{neato}$  (top) and  $DF_{opt}^{sfdp}$  (bottom) improvement over Neato and SFDP, respectively, on SuiteSparse14 graphs. Negative values favor  $DF_{opt}^{neato}$  and  $DF_{opt}^{sfdp}$ .

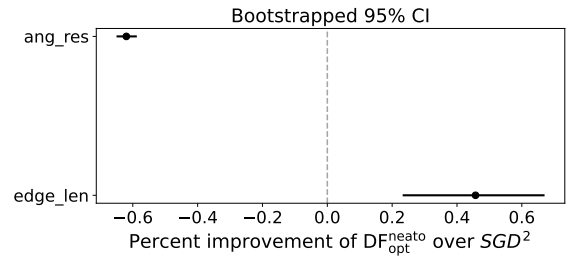
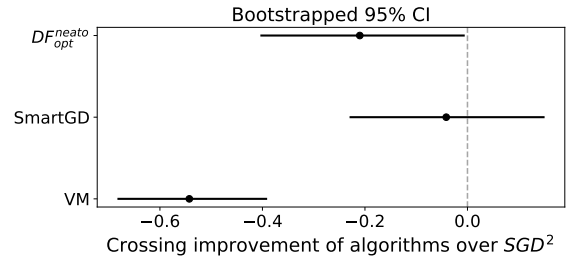


Fig. A2: (Top) Bootstrapped CIs for crossing improvement of algorithms compared to  $SGD^2$ . (Bottom) Bootstrapped CIs for  $DF_{opt}^{neato}$  improvement over  $SGD^2$  in angular resolution and edge length variation. Both on the Rome20 graphs.

Table A4: Optimal projections of the 10D  $sfdp$  layout. Numbers show  $sfdp$  vs.  $DF_{opt}^{sfdp}$  metrics. **Bold** = better. Edges colored by length: **red** = short, **blue** = long.

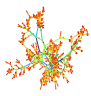
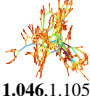
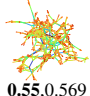
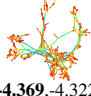
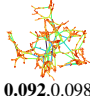
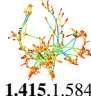
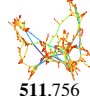
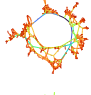
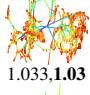
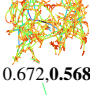
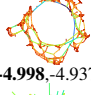
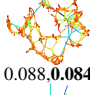
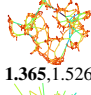

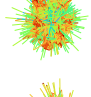

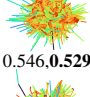
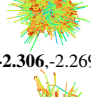
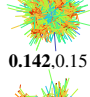
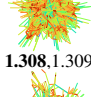

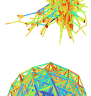

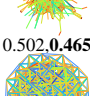
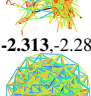



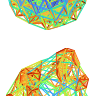
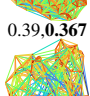
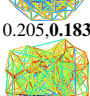
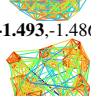
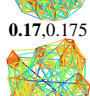


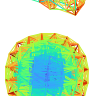
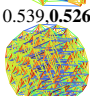
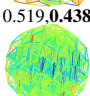
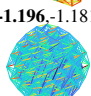
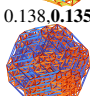

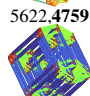
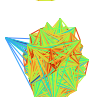
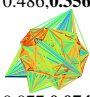
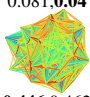
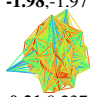
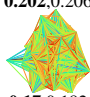
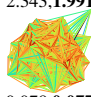
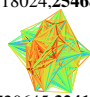

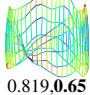

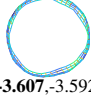
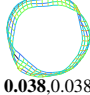
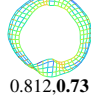
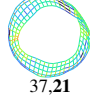
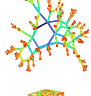
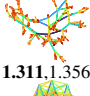
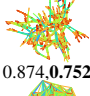
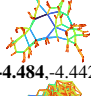
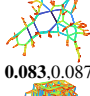
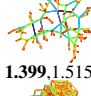

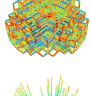
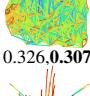
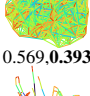

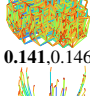
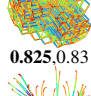

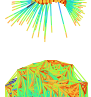
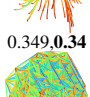
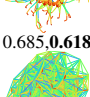

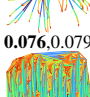
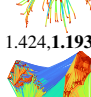
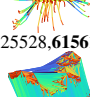
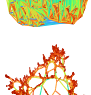
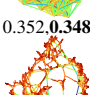
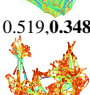
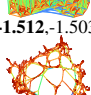
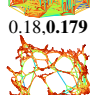
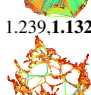


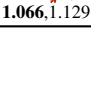
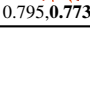
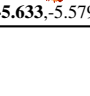
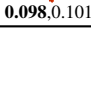
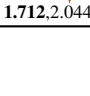
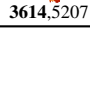







	$sfdp$	ang_res	edge_len	spr_elec	stress	tsne	xing
1138_bus							
		1.046,1.105	0.55,0.569	-4.369,-4.322	0.092,0.098	1.415,1.584	511,756
bcspwr07							
		1.033, <b>1.03</b>	0.672, <b>0.568</b>	-4.998,-4.937	0.088, <b>0.084</b>	1.365,1.526	678,1047
email							
		1.207, <b>1.097</b>	0.546, <b>0.529</b>	-2.306,-2.269	0.142,0.15	1.308,1.309	425417, <b>396344</b>
Erdos991							
		1.26, <b>1.183</b>	0.502, <b>0.465</b>	-2.313,-2.28	0.142, <b>0.131</b>	1.378, <b>1.334</b>	32632, <b>27123</b>
EX1							
		0.39, <b>0.367</b>	0.205, <b>0.183</b>	-1.493,-1.486	0.17,0.175	1.167, <b>1.089</b>	492441, <b>349871</b>
football							
		0.539, <b>0.526</b>	0.519, <b>0.438</b>	-1.196,-1.181	0.138, <b>0.135</b>	0.508, <b>0.507</b>	5622, <b>4759</b>
hypercube10							
		0.486, <b>0.356</b>	0.081, <b>0.04</b>	-1.98,-1.97	0.202,0.206	2.343, <b>1.991</b>	518024, <b>254686</b>
Journals							
		0.077, <b>0.074</b>	0.446,0.462	0.21,0.237	0.17,0.182	0.078, <b>0.077</b>	3720645, <b>3241000</b>
mobius							
		0.819, <b>0.65</b>	0.524, <b>0.193</b>	-3.607,-3.592	0.038,0.038	0.812, <b>0.73</b>	37,21
qh882							
		1.311,1.356	0.874, <b>0.752</b>	-4.484,-4.442	0.083,0.087	1.399,1.515	4337,5566
Si2							
		0.326, <b>0.307</b>	0.569, <b>0.393</b>	-1.568,-1.561	0.141,0.146	0.825,0.83	1242149, <b>1180389</b>
spiral							
		0.349, <b>0.34</b>	0.685, <b>0.618</b>	-2.857,-2.815	0.076,0.079	1.424, <b>1.193</b>	725528, <b>615614</b>
Trefethen_700							
		0.352, <b>0.348</b>	0.519, <b>0.348</b>	-1.512,-1.503	0.18, <b>0.179</b>	1.239,1.132	696237, <b>504843</b>
USpowerGrid							
		1.066,1.129	0.795, <b>0.773</b>	-5.633,-5.579	0.098,0.101	1.712,2.044	3614,5207

Table A5: Spring-electrical loss for SFDP layouts at different dimensions, vs that for the Optimal projection to 2D, and for the best PCA projection to 2D.

	sfdp at K					OptProj (from K-D to 2D)				PCA (from K-D to 2D)			
	2	3	5	7	10	3	5	7	10	3	5	7	10
1138_bus	-4.369	<b>-4.425</b>	-4.396	-4.362	-4.337	-4.417	-4.352	-4.374	-4.322	-4.415	-4.336	-4.339	-4.264
bcsppwr07	<b>-4.998</b>	-4.977	-4.970	-4.950	-4.852	-4.989	-4.992	-4.984	-4.937	-4.984	-4.984	-4.976	-4.918
email	-2.306	-2.368	-2.392	-2.402	<b>-2.406</b>	-2.274	-2.258	-2.262	-2.269	-2.273	-2.237	-2.227	-2.234
Erdos991	-2.313	-2.377	-2.369	<b>-2.392</b>	-2.389	-2.291	-2.260	-2.283	-2.280	-2.287	-2.227	-2.258	-2.235
EX1	-1.493	-1.606	-1.678	-1.700	<b>-1.701</b>	-1.487	-1.486	-1.486	-1.486	-1.476	-1.459	-1.469	-1.458
football	-1.196	-1.260	-1.292	<b>-1.294</b>	-1.285	-1.189	-1.188	-1.190	-1.181	-1.187	-1.182	-1.177	-1.172
hypercube10	-1.980	-2.084	-2.160	-2.192	<b>-2.203</b>	-1.966	-1.975	-1.973	-1.970	-1.961	-1.936	-1.909	-1.951
Journals	0.210	0.105	0.041	0.013	<b>-0.007</b>	0.225	0.246	0.238	0.237	0.228	0.260	0.272	0.282
mobius	<b>-3.607</b>	-3.606	-3.591	-3.590	-3.523	-3.605	-3.603	-3.605	-3.592	-3.596	-3.594	-3.594	-3.588
qh882	-4.484	<b>-4.493</b>	-4.473	-4.457	-4.446	-4.474	-4.459	-4.447	-4.442	-4.472	-4.454	-4.436	-4.429
Si2	-1.568	-1.628	-1.666	-1.679	<b>-1.686</b>	-1.566	-1.562	-1.562	-1.561	-1.566	-1.562	-1.561	-1.560
spiral	-2.857	<b>-2.865</b>	-2.828	-2.805	-2.819	-2.839	-2.799	-2.791	-2.815	-2.833	-2.786	-2.753	-2.761
Trefethen_700	-1.512	-1.608	-1.667	-1.692	<b>-1.703</b>	-1.502	-1.503	-1.504	-1.503	-1.492	-1.471	-1.411	-1.420
USpowerGrid	<b>-5.633</b>	-5.619	-5.593	-5.564	-5.532	-5.629	-5.614	-5.595	-5.579	-5.626	-5.609	-5.576	-5.573
SPC(sfdp)↓	0.000	-0.059	-0.090	-0.102	<b>-0.106</b>	0.009	0.018	0.015	0.017	0.011	0.028	0.036	0.039

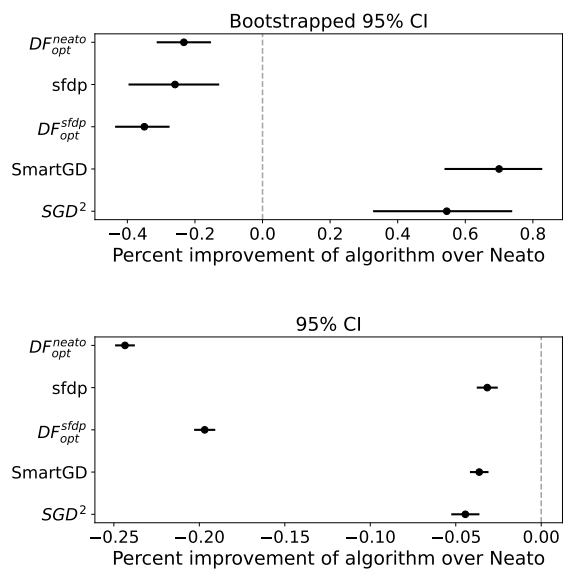


Fig. A3: (Top) Bootstrapped CIs for crossing improvement of algorithms compared to `neato`, on the 14 SuiteSparse graphs in our benchmark. (Bottom) Directly computed CIs across all Rome graphs for each algorithm's improvement over Neato in edge crossings.

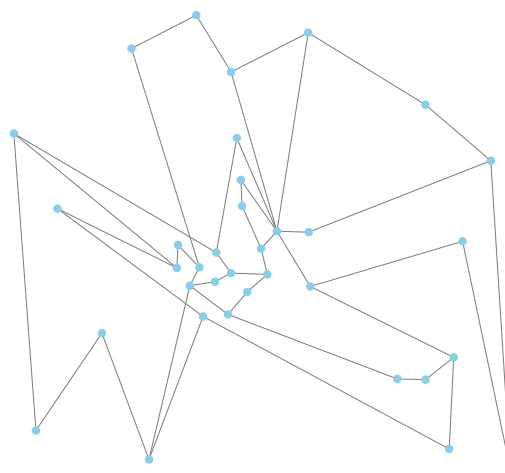


Fig. A4: Drawing of the rome graph grafo7023 obtained by the Vertex Movement algorithm. The drawing has a crossing number of 2, but ignores other aesthetic criteria. See Table A2 row 5, last column, for a drawing of the same graph by  $DF_{opt}^{neato}$ , which is aesthetically much more pleasing but with a crossing number of 8.

Table A6: Average variance explained for SuiteSparse14 graphs by PCA projection from 10D of two algorithms, with `sfdp` showing higher explained variance than `neato`. This suggests that minimum spring-electrical energy is better realized in lower dimensions than minimum stress energy.

Dimension	<code>neato</code>	<code>sfdp</code>
1	0.471	0.497
2	0.702	0.754
3	0.825	0.878
4	0.901	0.940
5	0.948	0.972

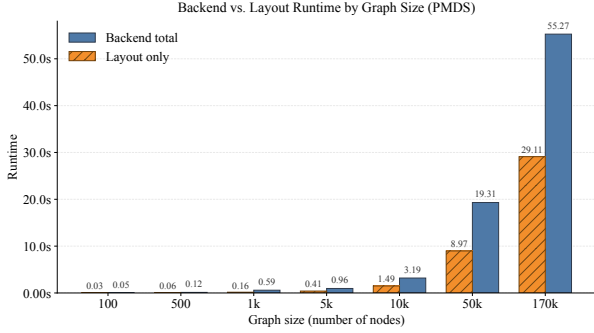


Fig. A5: Computation time comparison between Pivot MDS only and Pivot MDS + system processing

allowing users to explore the visualization and basic metrics immediately while more expensive metrics (e.g., t-SNE, edge crossings) are used as needed, keeping the system responsive and preventing blocking. Smart caching and cancellation further enhance usability: users can cancel in-progress jobs, toggle metric curves via the legend, and reuse cached results to avoid redundant work.

### A7 SCALABILITY OF THE SYSTEM

Built on `Three.js`, an OpenGL-based library, `DataFly` leverages GPU acceleration to enable smooth, real-time interaction with large graphs. On the backend, the server-side pipeline is also optimized for scalability. These, combined with scalable layout algorithms, e.g., `sfdp` or `PivotMDS`, allow `DataFly` to quickly visualize the layouts of large graphs. Figure A7 demonstrates the system rendering a 169K-node graph using the `sfdp` layout from four different viewpoints.

To quantitatively evaluate the practical scalability of our system, we measured both the total backend runtime and the time spent computing layouts across graphs of increasing size. We selected graphs from the SuiteSparse matrix collection, ranging from 115 to 170k nodes: football (115 nodes), Erdos991 (446 nodes), email (1133 nodes), USpower (4941 nodes), c-40 (9941 nodes), c-66 (49989 nodes) and c-73 (169422 nodes). Figure A5 and A6 show that layout computation dominates the overall runtime, especially for larger graphs. The gap between the total backend time and the layout-only time remains relatively modest compared with the layout cost itself, indicating that the main computational bottleneck lies in the layout generation procedure rather than in backend overhead. This suggests that the system is scalable to large graphs.

### A8 SYSTEM ITERATIVE IMPROVEMENTS AND FUTURE WORK

Expert E1 and non-expert N2 from the usability study suggested additional interaction features. E1 proposed automatic neighborhood highlighting (selecting a node and its immediate neighbors) and edge-based tracking through transitions, while N2 suggested a “lock-rotation” button and highlight-on-hover functionality.

In response, we have implemented several improvements in the live tool. A pause-and-resume function for animated transitions allows users to freeze the rotation at any viewpoint using the space key, supporting detailed inspection. Dynamic node and label highlighting, with enlargement on hover, improves visual clarity, particularly in dense projections.

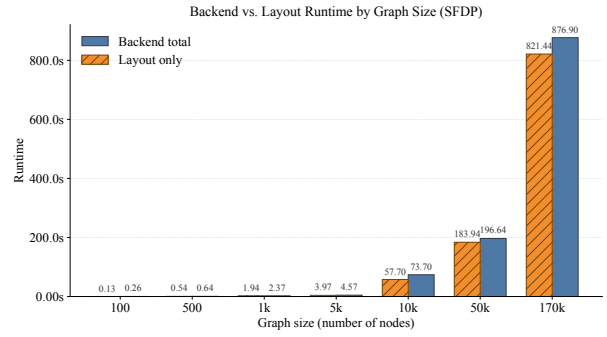


Fig. A6: Computation time comparison between `sfdp` only and `sfdp` + system processing

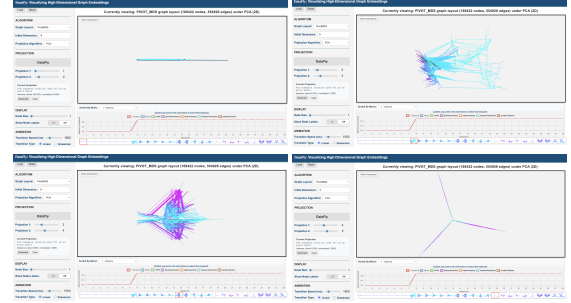


Fig. A7: The c-73 graph (169422 nodes, 554926 edges) from four viewpoints in `DataFly`.

Building on participant feedback, future work will further enhance interaction support, including ego-network and edge highlighting, to reduce manual effort during neighbor-tracing tasks. To bridge the gap between expert and non-expert users, we will introduce guided onboarding, contextual tool-tips, and progressive disclosure of advanced features to manage interaction complexity. Additionally, we plan to explore optimal “tours” between viewpoints—extending current linear or Grassmann geodesic transitions—to minimize both travel distance and a chosen quality metric (e.g., integrated stress), inspired by projection pursuit [13].

### A9 ADDITIONAL RELATED WORK

Our work connects to broader themes in graph and network visualization quality assessment. Bertini and Santucci [6] proposed a systematization of visual quality metrics for information visualization, classifying them into size, visual effectiveness, and feature preservation categories, justifying the principled use of quality metrics that we adopt for evaluating viewpoints. In a similar spirit, diagnostic approaches have been developed for specific visual representations: Gove [29] introduced *Gragnostics*, a set of fast, interpretable graph-level features for comparing graph topologies, while Behrisch et al. [4] proposed *Magnostics*, an image-based approach for ranking matrix views of networks according to the presence of visual patterns such as blocks and lines, and identified extending their diagnostics to hybrid representations such as *NodeTrix* [33] as future work. *NodeTrix*, introduced by Henry et al., combines node-link diagrams with adjacency matrices to simultaneously convey global network structure and local community detail, highlighting the long-standing challenge of representing dense substructures and reinforcing the case for our multi-view approach.